ESD-TR-81-255

MTR-8366

AD A108797

ANALYSIS OF MULTIPATH INTERFERENCE FOR APATS

By

G. A. ROBERTSHAW

DECEMBER 1981

Prepared for

DEPUTY FOR SURVEILLANCE AND CONTROL SYSTEMS
ELECTRONIC SYSTEMS DIVISION
AIR FORCE SYSTEMS COMMAND
UNITED STATES AIR FORCE
Hanscom Air Force Base, Massachusetts

DTIC FILE COPY

DTIC ELECTE DEC 1981 A

Approved for public release; distribution unlimited.

Project No. 4290

Prepared by

THE MITRE CORPORATION
Bedford, Massachusetts

Contract No. F19628-81-C-0001

When U.S. Government drawings, specifications, or other data are used for any purpose other than a definitely related government procurement operation, the government thereby incurs no responsibility nor any obligation whatsoever; and the fact that the government may have formulated, furnished, or in any way supplied the said drawings, specifications, or other data is not to be regarded by implication or otherwise, as in any manner licensing the holder or any other person or corporation, or conveying any rights or permission to manufacture, use, or sell any patented invention that may in any way be related thereto.

Do not return this copy. Retain or destroy.

REVIEW AND APPROVAL

This technical report has been reviewed and is approved for publication.

Michael Zymaris / GS-13
(Signature)
Michael Zymaris
Project Engineer/Scientist

FOR THE COMMANDER

(Signature)
EDWIN C. DOBKOWSKI, Lt Col, USAF
Systems Program Director, APATS

SECURITY CLASSIFICATION OF THIS PAGE (When Data Entered)

REPORT DOCUMENTATION PAGE

READ INSTRUCTIONS BEFORE COMPLETING FORM

1. REPORT NUMBER
ESD-TR-81-255

2. GOVT ACCESSION NO.
AD-A108 977

3. RECIPIENT'S CATALOG NUMBER

4. TITLE (and Subtitle)
ANALYSIS OF MULTIPATH INTERFERENCE FOR APATS

5. TYPE OF REPORT & PERIOD COVERED

6. PERFORMING ORG. REPORT NUMBER
MTR 8366

7. AUTHOR(s)
G. A. ROBERTSHAW

8. CONTRACT OR GRANT NUMBER(s)
F19628-81-C-0001

9. PERFORMING ORGANIZATION NAME AND ADDRESS
The MITRE Corporation
P. O. Box 208
Bedford, MA 01730

10. PROGRAM ELEMENT, PROJECT, TASK AREA & WORK UNIT NUMBERS
Project No. 4290

11. CONTROLLING OFFICE NAME AND ADDRESS
Deputy for Surveillance and Control Systems
Electronic Systems Division, AFSC
Hanscom Air Force Base, MA 01731

12. REPORT DATE
December 1981

13. NUMBER OF PAGES
70

14. MONITORING AGENCY NAME & ADDRESS (if different from Controlling Office)

15. SECURITY CLASS. (of this report)
UNCLASSIFIED

15a. DECLASSIFICATION/DOWNGRADING SCHEDULE

16. DISTRIBUTION STATEMENT (of this Report)
Approved for public release; distribution unlimited.

17. DISTRIBUTION STATEMENT (of the abstract entered in Block 20, if different from Report)

18. SUPPLEMENTARY NOTES

19. KEY WORDS (Continue on reverse side if necessary and identify by block number)
APATS
MULTIPATH
PROPAGATION
TELEMETRY

20. ABSTRACT (Continue on reverse side if necessary and identify by block number)

Multipath propagation and the resulting interference are theoretically analyzed for a ballistic missile re-entry vehicle (RV) to aircraft telemetry link in order to predict performance parameters for the ARIA Phased Array Telemetry System (APATS). A basic two-path model incorporating direct and specularly reflected transmission is presented. Model calculations, which take into account RV and APATS antenna gain, polarization, sea state and Doppler shift, yield the depth and frequency of fade

(over)

DD FORM 1 JAN 73 1473

UNCLASSIFIED

SECURITY CLASSIFICATION OF THIS PAGE (When Data Entered)

20. ABSTRACT (concluded).

anticipated for several mission scenarios. RF fades associated with RV antenna pattern nulls and modulation distortion resulting from a combination of Doppler shift and relative path delay are tentatively identified as the principal sources of link degradation which will limit APATS support altitudes. Areas of continuing interest and work are described.

ACKNOWLEDGMENTS

I am indebted to M. M. Weiner, J. D. R. Kramer, J. E. Roberts, and R. I. Millar for valuable discussions and expert guidance during the course of this work. I also wish to thank B. P. Nelson for reviewing the manuscript.

This report has been prepared by The MITRE Corporation under Project 4290. The contract is sponsored by the Electronic Systems Division, Air Force Systems Command, Hanscom Air Force Base, Massachusetts.

Accession For

A

TABLE OF CONTENTS

Section		Page
	LIST OF ILLUSTRATIONS	vi
1	INTRODUCTION - OBJECTIVES AND PRELIMINARY CONCLUSIONS	1
2	MODULATION DISTORTION	5
2.	UNMODULATED CARRIER WAVE	5
2.2	FREQUENCY MODULATED CARRIER WAVE	15
3	RF POWER FADING	20
4	CALCULATIONS	37
REFERENCES		53
APPENDIX A	RVCCS AZIMUTH DETERMINATION	55
APPENDIX B	RELATIVE GAIN OF RECEIVING ARRAY	59

LIST OF ILLUSTRATIONS

Figure		Page
1	Basic Multipath Model Geometry	6
2	Doppler Effect Geometry	8
3	Phasor Diagram	10
4	One Cycle of Amplitude Modulation	12
5	One Cycle of Phase Modulation	14
6	Doppler Shifted FM Spectrum	16
7	Basic Multipath Flat Earth Geometry	21
8	RV-Antenna Consolidated Coordinate System	26
9	Direct and Specular Rays Referenced to RVCCS	27
10	Illustration of Transformation to Horizontal Coordinate System	30
11	Direct and Specular Rays Referenced to Receiving Array Antenna	33
12	Time Delay Difference Vs. ARIA Altitude	38
13	Differential Doppler Shift Vs. ARIA Altitude	39
14	Model RV Antenna Gain Function	41
15	Simplified Local Coordinate System	42
16	RF Fade for Nearly Vertical RV Trajectory	43
17	RF Fade for Nearly Horizontal RV Trajectory	44
18	RF Fade for ARIA at 1 km Altitude	47
19	RF Fade for ARIA at 4 km Altitude	48
20	RF Fade for ARIA at 9 km Altitude	49
21	RF Fade Versus Sea State	50
22	RF Fade Versus Array Height (Receive Beamwidth)	52
23	Azimuth Difference Angle Versus ARIA Altitude for Several RV Trajectories, a 40 km Baseline, and RV Altitude of 1 km	57
24	2-Dimensional Array Geometry	60

SECTION 1

INTRODUCTION - OBJECTIVES AND PRELIMINARY CONCLUSIONS

The purpose of this study is to evaluate, from first principles, the character and severity of multipath propagation interference anticipated for the ARIA Phased Array Telemetry System (APATS). Earlier work[1] has identified multipath interference as the cause of link degradation at particular RV altitudes, and many present ARIA missions are constrained to wer altitudes for this reason. Flying the ARIA at relatively low altitudes (5000 ft. or less) is not desirable for several reasons and a means of alleviating multipath would be beneficial. To acquire a basic appreciation for the relevant parameters and essential relations needed to understand multipath problems, an elementary model is initially adopted, in which only two propagation paths or "channels" are considered.

The direct path is simply the line-of-sight from the re-entry vehicle (RV) to the ARIA. The second path is that of a ray which is reflected specularly and coherently by the sea surface below the transmitter and receiver. The diffuse or incoherent radiation which is scattered when reflection from a non-smooth surface occurs is ignored, save for the introduction of a "roughness factor" which approximately accounts for the attenuation of the reflected beam's coherent power. The motion of the RV causes different Doppler shifts of the transmitted waveform in the direct and specular directions, while the relative field strengths at the ARIA are a function of polarization, RV and ARIA antenna gains, reflection coefficients, and sea surface state, in the context of the RV-ARIA geometry. The interference of the two fields at the ARIA receiver has three principal manifestations which, although related, are usually discussed separately:

1) Power fading of the RF transmission due to destructive interference.

2) Distortion of the intelligence (baseband) modulated onto the carrier as a result of phase modulation of one channel's signal components by the others (intermodulation).

3) Intersymbol interference and intermodulation arising from the time delay difference of the two channels.

All of the above effects contribute to degradation of the link, and the relative strength of the contributing fields largely determines the extent of the deterioration.

The conclusions of this investigation to date, based on the elemetary model, include:

1) ARIA antenna directivity (3 db beamwidth of about 4°) minimizes serious multipath interference for RV altitudes greater than 2% of the RV-ARIA baseline (e.g., .8 km for 40 km baseline).

2) Under most circumstances, RF fades are significantly deeper for horizontal polarization since there is less reflection of the vertically polarized field by the sea.

3) For vertical polarization, there is an optimum RV-ARIA configuration which minimizes multipath, due to a reflection minimum in the specular channel at 6° grazing incidence (at S-band). Other considerations may outweigh the advantage gained by this configuration, however.

4) RF fading is less severe (neglecting RV antenna nulls) for higher receiver altitudes since the roughness factor and reflection coefficient amplitudes decrease with increasing grazing (specular) angle.

5) Channel time delay difference increases with ARIA and RV altitude and is approximately 1.5 μs at an ARIA altitude of 10.6 km (35,000 ft.), RV altitude of 1 km and 40 km RV-ARIA baseline.

6) The difference between the Doppler shifted frequencies of the direct and specular channels (differential Doppler) is dependent upon RV velocity, and for a given velocity increases with receiver altitude. Typically, values range up to 12 kHz for ARIA altitudes up to 10 km at a 40 km baseline separation.

7) Since the subcarrier frequencies used in the frequency division multiplex format (PCM/FM/FM) of the telemetry link are typically separated by 16 kHz and have 20 kHz bandwidth, differential Doppler can cause additional inter-subcarrier interference.

8) Assuming binary data rates of 10 kB/s per subcarrier, intersymbol interference is less than 4% in the multipath environment.

9) Multipath fades associated with RV antenna pattern nulls should be worst for RV trajectories with low penetration angles (measured with respect to the local horizontal) and, for a given trajectory, become more serious as the ARIA (APATS) altitude is increased.

These theoretical results suggest that the RV-ARIA multipath problem is associated with both the ARIA altitude dependence of the differential Doppler and the fades accompanying the RV antenna pattern nulls. Since relative channel delay increases with ARIA altitude, intersymbol interference may also lead to signal degradation for higher bit rates and ARIA altitudes.

Ongoing studies will include:

1) The impact of multipath on the PCM/FM and PCM/FM/FM telemetry format commonly used for RV-ARIA links.

2) Programmed calculations of RF fade using the experimental RV antenna gains.

3) The relative severity of multipath at P-band and S-band.

4) Link degradation arising from incoherent scattering and scintillation from the sea surface.

When a more complete comprehension of the multipath interference, as encountered in the context of APATS, is achieved, an investigation of alleviation techniques will follow.

In Section 2 the basic RV-ARIA geometry, Doppler effects, and FM waveform interference are considered. The details of the relationship between the RV antenna pattern, RV orientation, reflection coefficients, etc. which must be formulated to calculate the RF fade is presented in Section 3. Section 4 displays and discusses computer calculations based on the theory of Section 3. In the Appendices, details pertaining to the determination of azimuth in the RV coordinate system, and derivation of the APATS (phased array) antenna gain are presented.

SECTION 2

MODULATION DISTORTION

2.1 UNMODULATED CARRIER WAVE

In order to examine the basic problem of multipath interference in this telemetry link with as few complications as possible, this subsection treats the case of the interference between unmodulated carrier waves in the context of the two-channel model. In Figure 1, the basic geometry is illustrated. In addition to the direct "line-of-sight" path, only the coherent specular reflection path is considered. Despite the obvious simplicity of this model, several fundamental features of the multipath interference are exhibited. Consideration of important details such as RV and ARIA antenna patterns, surface reflection coefficients, state of the sea, etc. is deferred until a later section.

Since the RV speed (2-6 kms^{-1}) is always much greater than that of the ARIA (~0.2 kms^{-1}), it is reasonable to invoke an approximation in which the ARIA is stationary. Since the receiver (e.g. APATS) is always in the far field of the RV antenna, the field at the receiver may be considered as the sum of plane waves arriving from the line-of-sight and specular directions. If the transmitted carrier wave has angular frequency ω_o, the phase of the direct and specular waves, referenced to a time, t_o, is given by,

$$\phi_D = \vec{k}_D \cdot \vec{D} - \omega_o (t-t_o) \tag{1a}$$

$$\phi_S = \vec{k}_S \cdot \vec{S} - \omega_o (t-t_o) + \phi_F \tag{1b}$$

in which the vectors $\vec{D}$ and $\vec{S}$ are functions of time.

IA-62,002

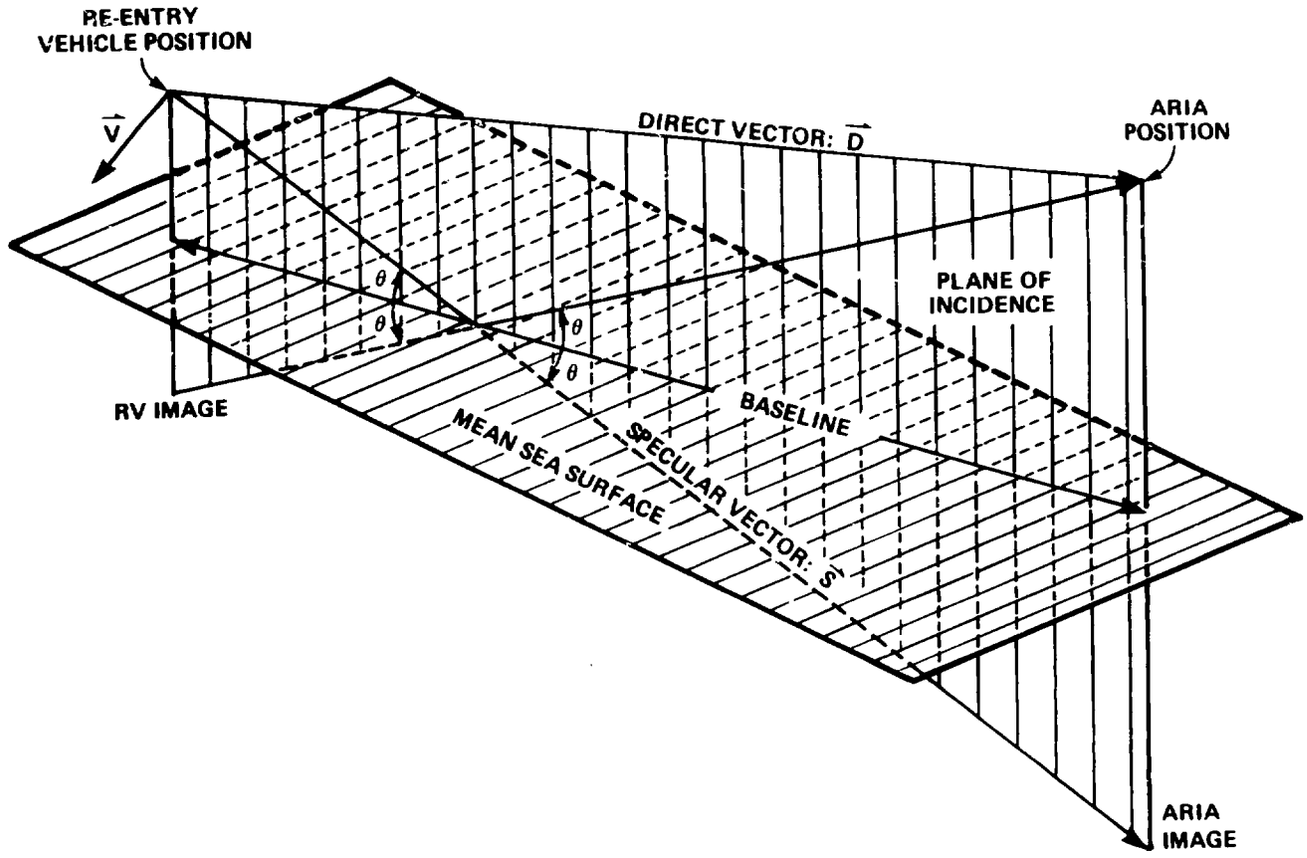

Figure 1. BASIC MULTIPATH MODEL GEOMETRY

$$\vec{D}(t) = \vec{D}_{t_o} - \vec{V}\,(t-t_o) \tag{2a}$$

$$\vec{S}(t) = \vec{S}_{t_o} - \vec{V}\,(t-t_o) \tag{2b}$$

and the propagation vectors are given by,

$$\vec{k}_D = \frac{\omega_o}{c}\,\hat{D} \tag{3a}$$

$$\vec{k}_S = \frac{\omega_o}{c}\,\hat{S} \tag{3b}$$

in which $\hat{D}$ and $\hat{S}$ are unit vectors in the line-of-sight and specular directions respectively, as illustrated in Figure 2, and the time dependence of the unit vectors has been neglected. The constant phase shift, Φ_F, is associated with reflection of the specular ray from the sea. The velocity is assumed to be constant over the time interval $t-t_o$, which is a fair approximation for $t-t_o<10^{-1}$s--a time which is very large relative to the carrier period ($\sim 10^{-9}$s) or path delay time difference ($\sim 10^{-6}$ sec) in the multipath environment.

Substitution of Equations (2) and (3) into Equation (1) yields,

$$\Phi_D = \frac{\omega_o |\vec{D}_{t_o}|}{c} - \omega_o \left(1 + \frac{\vec{V}\cdot\hat{D}}{c}\right)(t-t_o) \tag{4a}$$

$$\Phi_S = \frac{\omega_o |\vec{S}_{t_o}|}{c} - \omega_o \left(1 + \frac{\vec{V}\cdot\hat{S}}{c}\right)(t-t_o) + \Phi_F \tag{4b}$$

From which it is evident that the relative motion of the source and receiver produces Doppler shifts of the carrier, which, for this non-relativistic treatment are, more explicitly,

IA-62,003

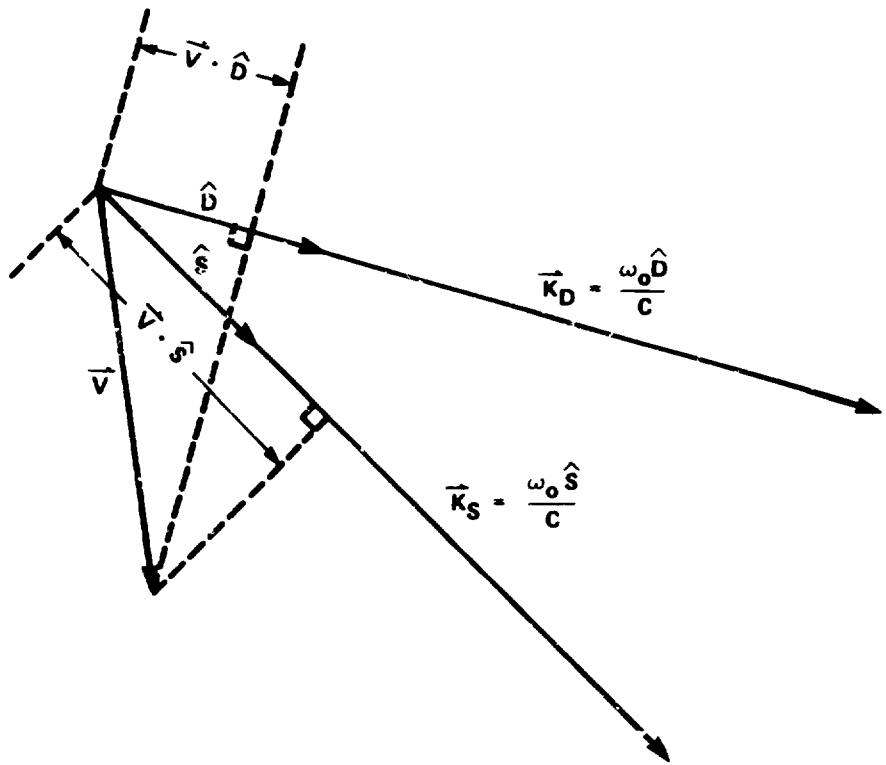

Figure 2. DOPPLER EFFECT GEOMETRY

$$D_D\omega_o = (1 + \frac{\vec{V} \cdot \hat{D}}{c})\,\omega_o \tag{4c}$$

$$D_S\omega_o = (1 + \frac{\vec{V} \cdot \hat{S}}{c})\,\omega_o \tag{4d}$$

in which D_D and D_S are Doppler factors in the direct and specular directions respectively. The size of the Doppler shift is a linear function of the projection of the RV velocity on the direction of observation, as might be anticipated. Since the RV velocity, and $\hat{D}$ and $\hat{S}$ are time dependent, the Doppler factors will vary as the RV descends; however, this variation is very slow compared to the carrier wave period or relative channel delay times, and the approximations which led to Equations (4c) and (4d) are acceptable.

If constant phase shifts, which do not materially affect the result, are neglected, the waveform received by APATS can be expressed as a phasor sum of the voltages associated with the direct and specular fields, designated V_D and V_S respectively. Thus, the resultant voltage V_R is given by,

$$V_R(t) = \mathrm{Re}\,[V_D\, e^{i(D_D\omega_o t)} + V_S\, e^{i(D_S\omega_o t)}] \tag{5}$$

and the amplitude of V_D relative to V_S will be considered in detail in the next section. Equation (5) is represented vectorily in Figure 3. The direct field voltage phasor rotates at angular frequency $D_D\omega_o$, while the specular field vector rotates relatively slowly around it at angular frequency $\omega_o(D_S-D_D)$. Equation (5) can be re-expressed in terms of the amplitude and phase of the resultant:

$$V_R(t) = \left[V_D^2 + V_S^2 + 2V_DV_S \cos\left(\omega_o\,(D_S-D_D)t\right)\right]^{1/2} \times \cos\left[\omega_o\, D_D\, t + \alpha\right] \tag{6}$$

IA-62,004

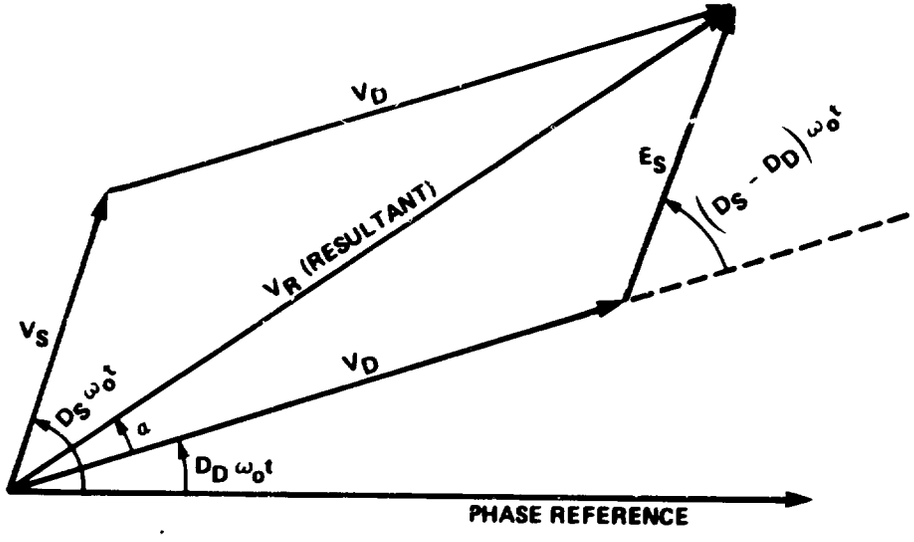

Figure 3. PHASOR DIAGRAM

$$\alpha = \mathrm{TAN}^{-1}\left[\frac{V_S \ \mathrm{SIN}\ (\omega_o(D_S-D_D)t)}{V_D + V_S \ \mathrm{COS}\ (\omega_o\ (D_S-D_D)t)}\right] \tag{7}$$

Examination of Eqs. (6) and (7) reveals that the resultant field is both amplitude and phase modulated. In both cases the frequency of the modulation is the differential Doppler frequency, ω_{DD}:

$$\omega_{DD} = \omega_o\ (D_S-D_D) \tag{8}$$

also referred to as the "beat frequency" in the context of the addition of two pure tones of slightly different frequency.

A plot of the normalized voltage amplitude versus phase (time) is shown in Figure 4, and from Eq. (6) it is seen that:

$$\begin{cases} V_{RMAX} = V_D + V_S \ ; \quad t = \dfrac{2n\pi}{\omega_{DD}} \\ V_{RMIN} = V_D - V_S \ ; \quad t = \dfrac{(2n+1)\pi}{\omega_{DD}} \end{cases} \qquad n = 0,\ 1,\ 2,\ \ldots \tag{9}$$

the amplitude modulation factor:

$$A(t) = [V_D^2 + V_S^2 + 2V_DV_S \ \mathrm{COS}(\omega_{DD}t)]^{1/2} \tag{10}$$

is also referred to as an envelope function.

The phase of the resultant voltage, $V_R(t)$, is, from Eq. (6),

$$\phi_R(t) = \omega_o\ D_Dt + \mathrm{TAN}^{-1}\left[\frac{V_S \ \mathrm{SIN}\ (\omega_{DD}t)}{V_D + V_S \ \mathrm{COS}\ (\omega_{DD}t)}\right] \tag{11}$$

and in order to determine the instantaneous frequency of the total voltage, it is necessary to differentiate the phase with respect to time:

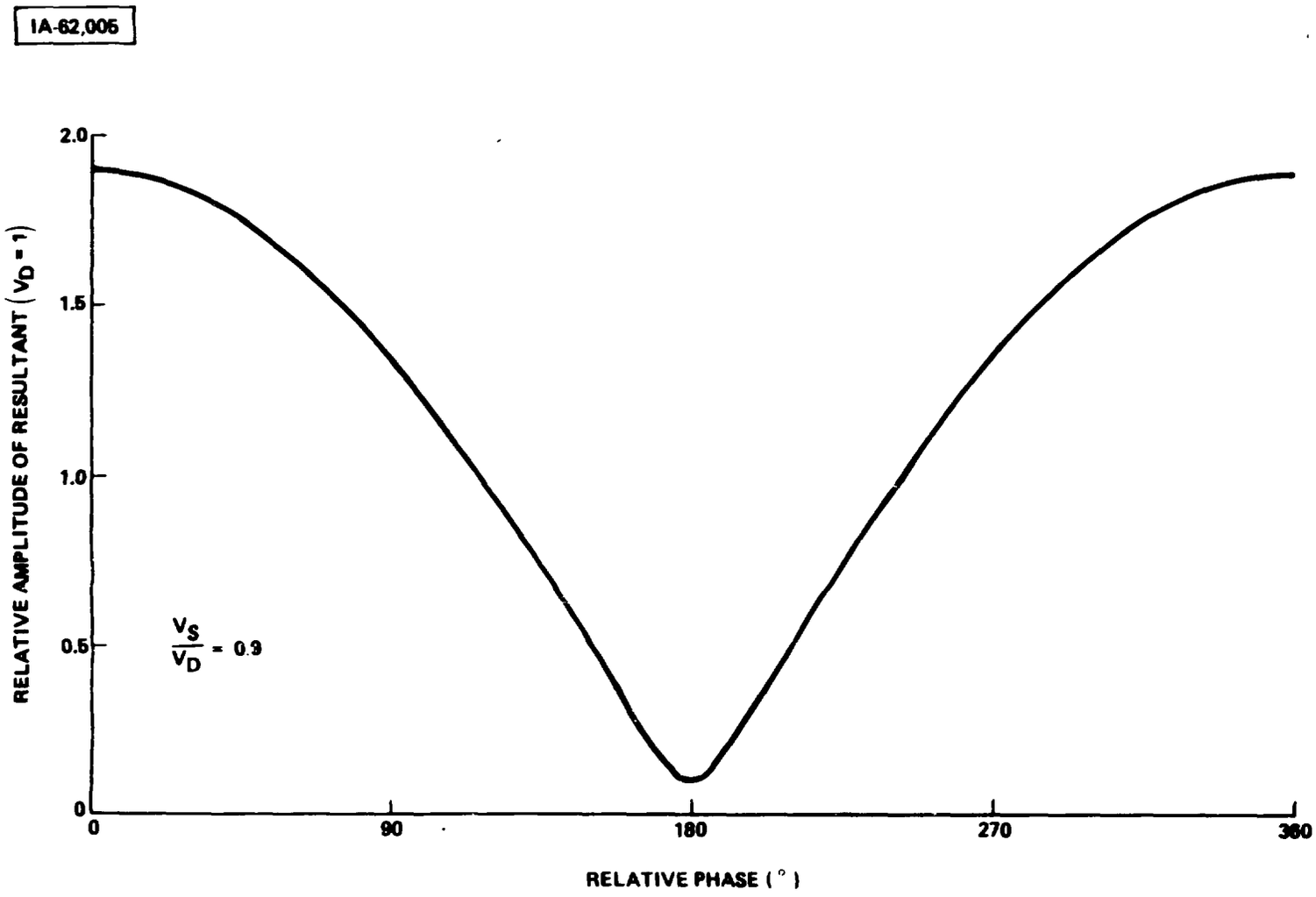

Figure 4. ONE CYCLE OF AMPLITUDE MODULATION

$$\omega_R(t) = \frac{d\phi_R(t)}{dt} = \omega_o D_o + \omega_{DD}\left[\frac{V_D V_S \cos(\omega_{DD}t) + V_S^2}{V_S^2 + V_D^2 + 2 V_S V_D \cos(\omega_{DD}t)}\right] \quad (12)$$

A plot of the frequency deviation, i.e., the right-hand term on the right-hand side of Eq. (12), is given in Figure 5, using the same parameters as employed in Figure 4; $V_s/V_D = 0.9$, $\omega_{DD} = 10$ kHz. The frequency maxima and minima are:

$$\begin{cases} \omega_{RMAX} = \omega_o D_D + \omega_{DD}\left[\frac{V_S}{V_S+V_D}\right]; \; t = \frac{2n\pi}{\omega_{DD}} \\ \omega_{RMIN} = \omega_o D_D - \omega_{DD}\left[\frac{V_S}{V_D-V_S}\right]; \; t = \frac{(2n+1)\pi}{\omega_{DD}} \end{cases} \quad n = 0, 1, 2 \ldots \quad (13)$$

A measure of the width of the deep valley in the frequency deviation function is obtained from the "zero-crossing" points:

$$\omega_R = \omega_o D_D; \text{WHEN } t = \frac{(2n+1)\pi}{\omega_{DD}} \pm \left|\frac{\cos^{-1}\left[\frac{V_S}{V_D}\right]}{\omega_{DD}}\right|; n = 0, 1, 2 \ldots . (14)$$

and the fraction of time during which the deviation is negative is:

$$T(\omega_R < \omega_o D_D) = \frac{1}{\pi}\left|\cos^{-1}\left(\frac{V_S}{V_D}\right)\right|$$

For example, if V_s/V_D is 0.9, the freq. deviation is negative 14% of the time. Note that as V_S approaches V_D in magnitude, the negative deviation becomes much greater while its duration decreases. The deviation can be expressed in terms of its fourier components:[2]

$$\omega_{DEV}(t) = \omega_{DD} \sum_{n=1}^{\infty} (-1)^{n+1}\left(\frac{V_S}{V_D}\right)^n \cos(n\omega_{DD}t) \quad (15)$$

The fundamental frequency modulation term has the Doppler beat frequency, ω_{DD}, while all harmonics have amplitudes proportional to ω_{DD}. There is no constant term, and therefore the average freq. deviation is zero. Note that as V_S approaches V_D, the series

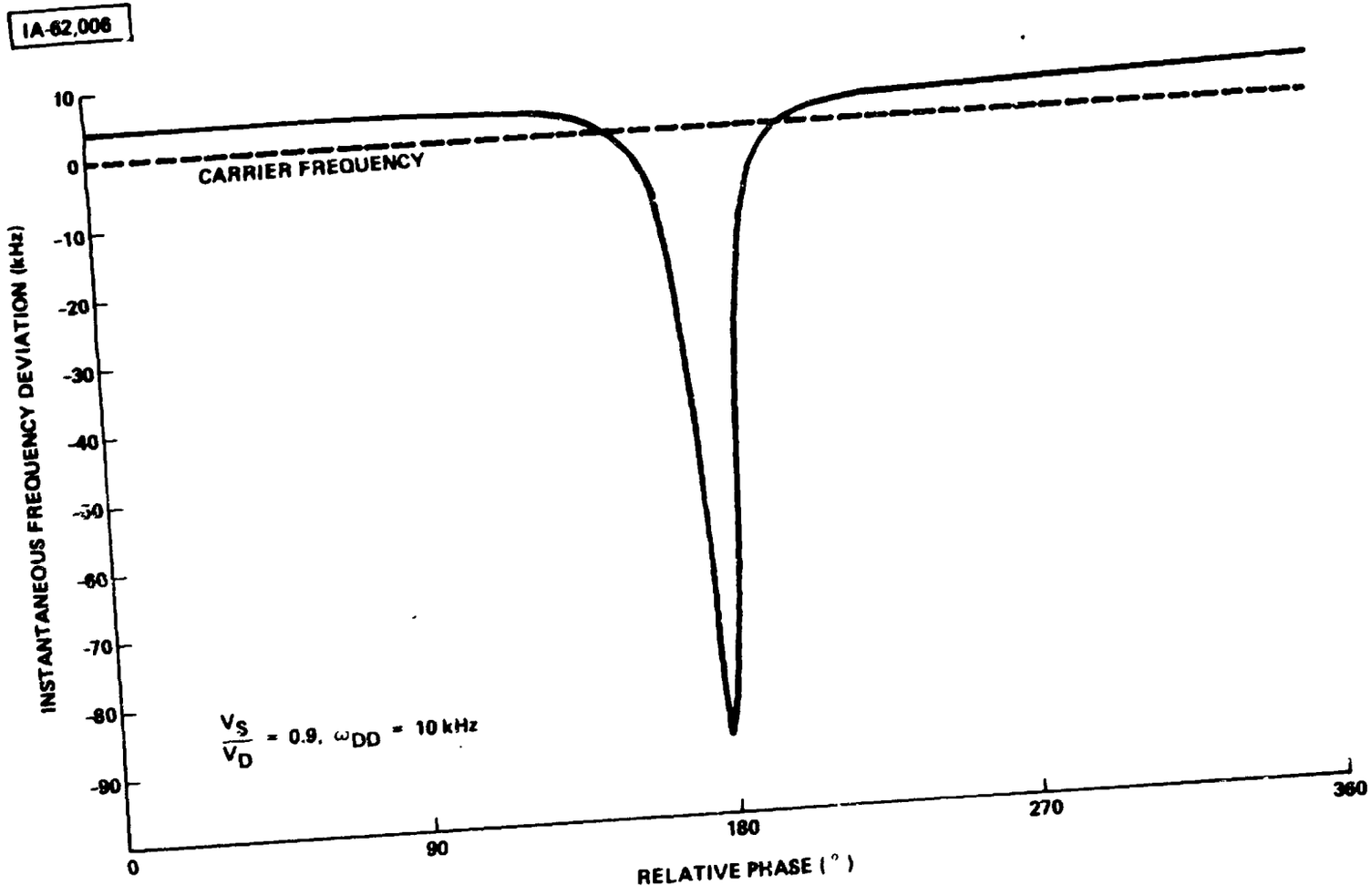

Figure 5. ONE CYCLE OF PHASE MODULATION

converges slowly and many terms contribute significantly to the overall deviation.

The frequency spectrum of the amplitude limited resultant for this case,

$$V_R = \{\text{const}\} \cos [\phi_R(t)]$$

is very complicated and spread out, and has been considered in detail elsewhere.[3] Consideration of this spectrum is necessary in connection with the function of the limiter component of an FM detector, which ideally eliminates the amplitude modulation represented by Eq. (10). Thus far, only interference between unmodulated carriers has been considered. However, it is already apparent that potentially large amplitude and frequency variations which have been examined here can have a deleterious effect on the RV-ARIA telemetry link.

2.2 FREQUENCY MODULATED CARRIER WAVE

For simplicity, consider the carrier to be frequency modulated by a single sinusoidal component. On the RV the instantaneous frequency is,

$$\omega(t) = \omega_o + k_1 \cos (\omega_1 t) \tag{15}$$

in which ω_1 is the modulation (baseband) frequency and k_1 is the maximum frequency deviation. The Doppler shift of frequency modulated transmission is illustrated in Figure 6, which shows how the spectral components are scaled by the Doppler factor, D . The particular wideband FM spectrum shown is only schematic, but it should be noted that before Doppler shifting, the adjacent

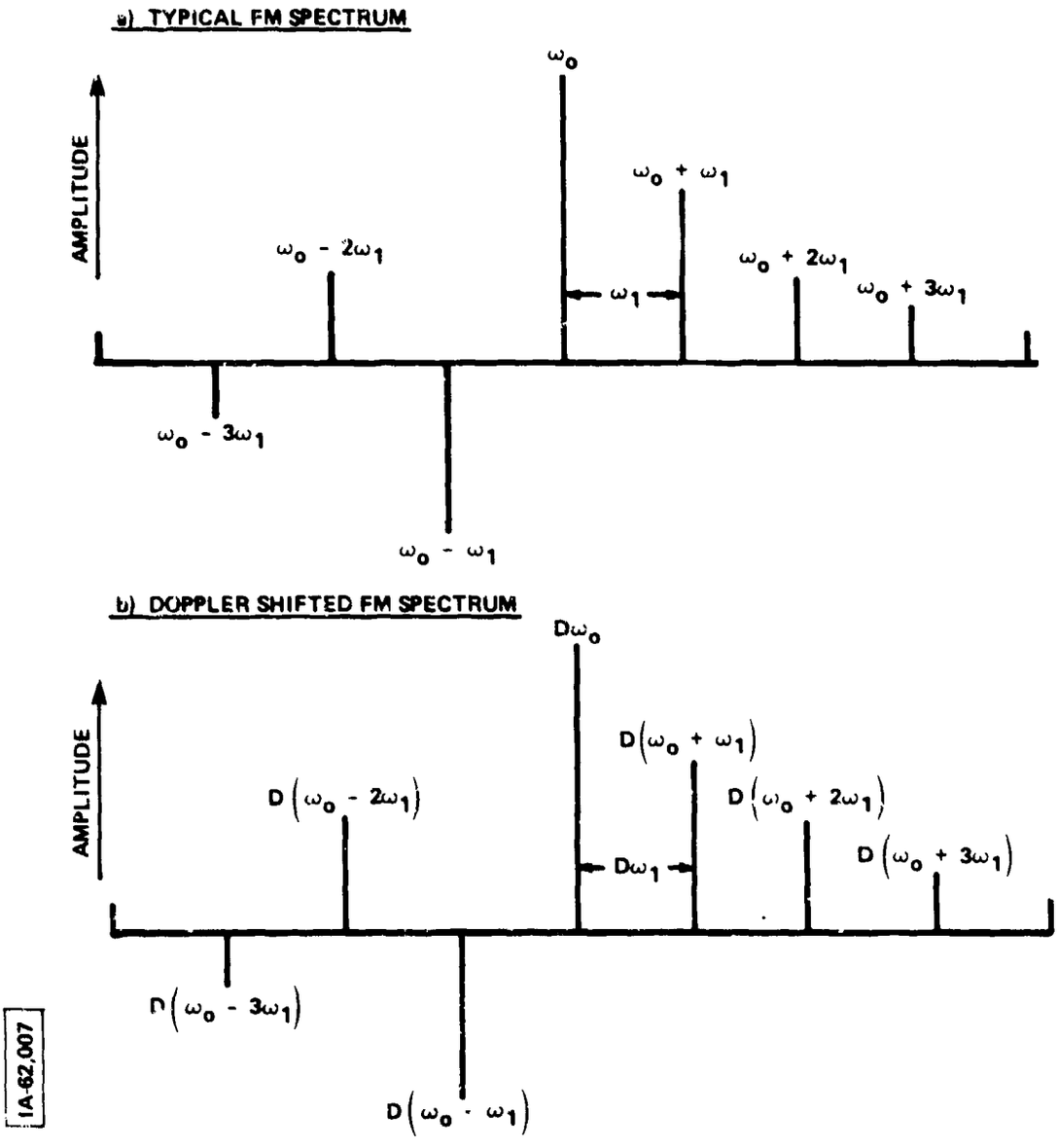

Figure 6. DOPPLER SHIFTED FM SPECTRUM

components are separated by ω_1 ; however, after Doppler shifting the separation is $D\omega_1$, indicating that the Doppler-shifted modulation frequency is $D\omega_1$ as expected. Therefore, because of the Doppler shift and transit time delays, τ_D and τ_S, the frequency of the direct path wave at the receiving point (ARIA) may be expressed:

$$\omega_D(t) = D_D\omega_o + D_D k_1 \cos [D_D\omega_1 (t-\tau_D)] \tag{17}$$

Similarly, for the specular path wave:

$$\omega_s(t) = D_s\omega_o + D_s k_1 \cos [D_s\omega_1 (t-\tau_s)] \tag{18}$$

Integration of these equations with respect to time yields the phases of the respective waves,

$$\Phi_D(t) = \int \omega_D(t)\, dt = D_D\omega_o t + \beta_1 \, \mathrm{SIN}(D_D\omega_1(t-\tau_D)) \tag{19}$$

$$\Phi_S(t) = \int \omega_S(t)\, dt = D_S\omega_o t + \beta_1 \, \mathrm{SIN}(D_S\omega_1(t-\tau_S)) + \phi_o \tag{20}$$

in which $\beta_1 = k_1/\omega_1$ is the modulation index and the integration constants have been combined in ϕ_o . Note that the Doppler shifts do not change the modulation index, which is consistent with Figure 6. For convenience,

$$\Phi(t) = \Phi_S(t) - \Phi_D(t)$$

is the phase difference between the direct and specular voltages. The voltages may be expressed,

$$v_D(t) = \cos(\Phi_D(t)) \tag{21}$$

$$v_s(t) = \rho \cos (\Phi_s(t)) \tag{22}$$

in which, $\rho = \frac{V_S}{V_D}$

is the ratio of the voltage amplitudes. Phasor addition of the fields yields:

$$v_R(t) = v_D(t) + v_s(t) = [1 + \rho^2 + 2\rho \cos \Phi(t)]^{1/2} \cos [\Phi_D(t)+\theta] \quad (23)$$

$$\theta = \mathrm{TAN}^{-1} \left[\frac{\rho \mathrm{SIN}\, \Phi(t)}{1 + \rho \mathrm{COS}\, \Phi(t)}\right] \quad (24)$$

The instantaneous angular frequency of the resultant wave is given by:

$$\omega_R(t) = \frac{d\Phi_D(t)}{dt} + \frac{d\theta}{dt} \quad (25)$$

The first term is just the desired signal which would be detected if no interfering wave were present. Elsewhere[2] it has been shown that the distortion term, θ, has the expansion:

$$\theta(t) = \sum_{n=1}^{\infty} \frac{(-1)^{n+1}}{n} \rho^n \mathrm{SIN}\ (n\Phi(t)) \quad (26)$$

Examination of one term reveals:

$$\sin [n\, \Phi(t)] = \mathrm{Im}\ [e^{in\Phi(t)}] \quad (27)$$

$$= \mathrm{Im} \left[e^{in\left[D_S\omega_o t - D_D\omega_o t + \beta_1 \left(\mathrm{SIN}(D_S\omega_1(t-\tau_S)) - \mathrm{SIN}(D_D\omega_1(t-\tau_D))\right)+\phi_o\right]} \right]$$

At this point, it is worthwhile to introduce the standard expansion,

$$e^{ia\sin\omega t} = \sum_{n=-\infty}^{\infty} J_n(a)\ e^{in\omega t} \quad (28)$$

in which $J_n(a)$ is the Bessel function of the first kind and order n. With this the expression for θ below is obtained,

$$\theta(t) = \sum_{n=1}^{\infty} \frac{(-1)^{n+1}}{n} \rho^n \sum_{m=-\infty}^{\infty} J_m(n\beta_1) \sum_{k=-\infty}^{\infty} J_k(n\beta_1) \times \tag{29}$$

$$\mathrm{SIN}\left[\left(n\omega_{DD} + \left(mD_S - kD_D\right)\omega_1\right) t + \omega_1\left(kD_D\tau_D - mD_S\tau_S\right) + n\phi_o\right]$$

where, as before $\omega_{DD} = (D_S - D_D)\,\omega_o$.

The frequency distortion is given by the time derivative of θ:

$$\frac{d\theta}{dt} = \sum_{n=1}^{\infty} \frac{(-1)^{n+1}}{n} \rho^n \sum_{m=-\infty}^{\infty} J_m(n\beta_1) \sum_{k=-\infty}^{\infty} J_k(n\beta_1) \times \tag{30}$$

$$(n\omega_{DD} + mD_S\omega_1 - kD_D\omega_1)\ \mathrm{COS}\ [(n\omega_{DD} + mD_S\omega_1 - kD_D\omega_1)\ t +$$

$$\omega_1(kD_D\tau_D - mD_S\tau_S) + n\phi_o]$$

Once again, it should be remembered that the time dependence of D_D, D_s, τ_D and τ_s has been suppressed since changes in these quantities are slow relative to the modulation period. Unless $\omega_{DD} = 0$, in general no distortion component will occur at the same frequency as the Doppler-shifted baseband modulation, $D_1\omega_1$. However, it is quite feasible for distortion components to fall within the passband of the low pass filter which usually follows the discriminator in a typical FM receiver, and such components will contribute to noise. The well known signal to noise improvement and co-channel interference rejection capabilities of wideband FM will mitigate against multipath and a detailed examination of these subjects should be performed.

SECTION 3

RF POWER FADING

In Section 2 the general character of the interference which can occur in the context of the two-channel multipath model was explored. In particular, it was shown that the resultant waveform is both amplitude and phase modulated (Eqs.6,11). The relative strengths of the interfering voltages determine the extremes of the amplitude modulation (Eq. 9) and instantaneous frequency excursion (Eq. 13). It is therefore essential, for any practical investigation of signal degradation arising from multipath interference, to estimate the relative strengths of the direct and specular fields and the respective voltages at the output of the receiving antenna. This is the subject of this section.

All of the factors which must be considered to determine the relative field strength must be examined in the context of the RV-ARIA geometry, shown exaggerated in Figure 7. When the RV and ARIA altitudes, and RV-ARIA range are small in comparison with the radius of the earth, R_e, a flat earth approximation can be employed without incurring serious errors. The direct path vector from the RV to the ARIA, $\vec{D}$, is given by,

$$\vec{D} = \vec{R}_A - \vec{R}_V \tag{31}$$

and the specular path vector from the RV to the ARIA image is given by,

$$\vec{S} = (1-2r_A)\,\vec{R}_A - \vec{R}_V + \frac{2r_c\,\vec{R}_c}{|\vec{R}_c|} \tag{32}$$

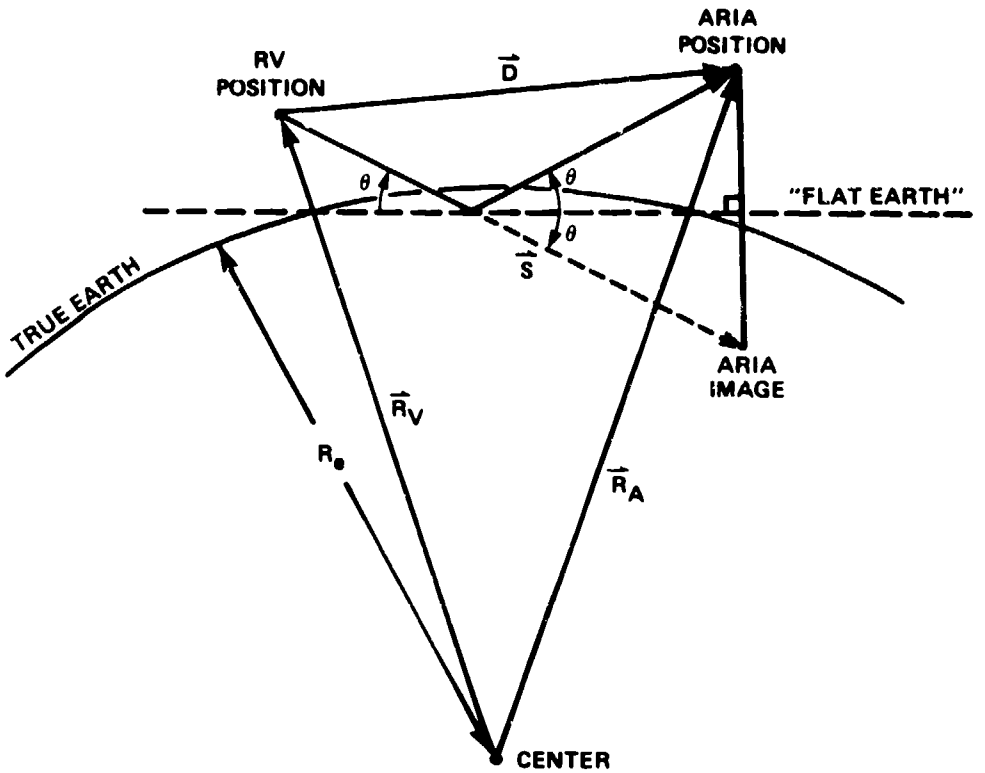

IA-62,008

Figure 7. BASIC MULTIPATH FLAT EARTH GEOMETRY

where,

$$r_A = \frac{R_e}{|\vec{R}_A|} \quad ; \vec{R}_C = r_A \vec{R}_A - r_V \vec{R}_V$$

$$r_C = \frac{\vec{R}_C \cdot (1-r_A)\vec{R}_A}{|\vec{R}_C|}$$

and,

$$r_V = \frac{R_e}{|\vec{R}_V|}$$

Thus, a relative space loss factor is immediately obtainable:

$$r_{SL} = \left(\frac{|\vec{D}|}{|\vec{S}|}\right)^2 \tag{33}$$

The specular beam is also attenuated as a result of reflection from the sea. The specular angle, θ, which is measured in the plane of incidence with respect to the horizontal is given by,

$$\theta = \mathrm{TAN}^{-1}\left[\frac{\left[(1-r_A)\vec{R}_A + (1-r_V)\vec{R}_V\right]\dfrac{r_A\vec{R}_A + r_V\vec{R}_V}{r_A\vec{R}_A + r_V\vec{R}_V}}{|\vec{R}_C| + \hat{R}_C \cdot \left[(r_V-1)\vec{R}_V + (1-r_A)\vec{R}_A\right]}\right] \tag{34}$$

The Fresnel reflection coefficients for reflection from a smooth surface are a function of θ, incident field polarization, and surface conductivity and dielectric constant[4];

$$\alpha_R^H = \left|\alpha_R^H e^{i\delta_R^H}\right| = \left|\frac{\mathrm{SIN}\,\theta - (\eta^2 - \mathrm{COS}^2\theta)^{1/2}}{\mathrm{SIN}\,\theta + (\eta^2 - \mathrm{COS}^2\theta)^{1/2}}\right| \tag{35}$$

$$\alpha_R^V = \left|\alpha_R^V e^{i\delta_R^V}\right| = \left|\frac{\eta^2\ \mathrm{SIN}\,\theta - (\eta^2 - \mathrm{COS}^2\theta)^{1/2}}{\eta^2\ \mathrm{SIN}\,\theta + (\eta^2 - \mathrm{COS}^2\theta)^{1/2}}\right| \tag{36}$$

In the above, the superscript H denotes horizontal polarization, while V denotes vertical (in plane of incidence) polarization, and η^2 is the complex dielectric constant,

$$\eta^2 = \epsilon_r - i \frac{(18\text{x}10^3)\sigma}{\text{freq.(MHz)}} \tag{37}$$

For sea water[5], the relative (to air) dielectric const, ϵ_r, and conductivity σ are:

$$\epsilon_r = 81 \quad ; \quad \sigma \cong 4 \quad \text{MHO/M}$$

The reflection coeff. for horizontal polarization, α_R^H, is close to unity for $0 < \theta < 30^\circ$, but the reflection coeff. for vertical polarization, α_R^V, goes through a minimum of about 0.1 at $\theta \simeq 6^\circ$ (Brewster angle).

If the sea-surface is not absolutely smooth, the amplitude of the specular component for both polarizations is reduced by an additional factor upon reflection, which has the root mean square value[6],

$$(\alpha_{SS})_{RMS} \cong \exp\left[-8\pi^2 \left(\frac{\sigma_h \text{ SIN}\,\theta}{\lambda}\right)^2\right] \tag{38}$$

in which σ_h is the standard deviation of the wave height about the mean surface, and λ is the wavelength of the incident radiation. The above equation for α_{SS} is exact if the surface height is a random variable with a Gaussian probability distribution. Experimentally[7], it is found that Eq. (38) provides a good approximation for reflection from an actual sea surface if,

$$\frac{\sigma_h \text{ SIN}\,\theta}{\lambda} \leq 0.1 \tag{39}$$

If this condition is not satisfied, Eq. (38) underestimates the amplitude of the coherently reflected field. A sea state number and description has been associated with certain ranges of σ_h values[8]. Obviously, as the surface "roughness" increases, more of the incident wave is scattered incoherently over a range of directions.

Two very important factors, which have not been taken into account yet are, (1) the RV antenna gain (transmission) and (2) the ARIA phased array antenna gain (reception). The RV antenna typically consists of two circumferential wave guide slots on opposite sides of the RV and fed in phase electrically. This arrangement is intended to alleviate severe shadowing which would otherwise occur as a result of RV rotation (nominally 4π radians/sec). The far field radiation pattern from the RV is very complex and cannot be conveniently described analytically[9]. It is therefore necessary to directly measure the RV radiation pattern using equipment designed for this purpose. To fully characterize the field with adequate resolution, the following quantities, measured at 2° angular increments in elevation and azimuth, are sufficient;

<u>Alternative 1:</u>

a) linear component amplitude (gain),
b) orthogonal linear component amplitude,
c) phase angle between components (e.g. a) leads b) by δ°)

<u>Alternative 2:</u>

a) right hand circular component amplitude,
b) left hand circular component amplitude,
c) phase angle between circular components.

Other alternatives are possible, but basically three independent quantities must be measured. By convention, all measurements are made with reference to the RV-antenna consolidated coordinate system[9] (RVCCS), which is rigidly fixed to the RV with its polar axis coincident with the RV roll axis, as shown in Figure 8. At RV altitudes relevant for APATS, i.e., less than 125 km, the RV velocity vector is parallel to the RV roll axis (negligible wobble). RV orientation, with respect to the ARIA, is characterized by its velocity vector direction and rotational position about its roll axis. The angles between the vectors $\vec{D}$ and $\vec{V}$, and $\vec{S}$ and $\vec{V}$, correspond to the elevation coordinates in RVCCS of the direct and specular emission directions, respectively. These angles are readily obtained:

$$\theta_D(t) = \cos^{-1} [\hat{V}(t) \cdot \hat{D}(t)] \tag{40}$$

$$\theta_S(t) = \cos^{-1} [\hat{V}(t) \cdot \hat{S}(t)] \tag{41}$$

The azimuth angles in RVCCS are measured from an arbitrary reference azimuth in a counter-clockwise direction as one views the nose of the RV. (See Figures 8 and 9.) If the RV rotates with an angular velocity ω_{RV} and does not change the direction of its velocity, the direct and specular ray azimuths in the RVCCS are given by,

$$\phi_D(t) = \phi_D(t_o) \pm \omega_{RV}(t-t_o) \tag{42}$$

$$\phi_S(t) = \phi_D(t) - \Delta \tag{43}$$

in which $\phi_D(t_o)$ is the RVCCS azimuth value of $\vec{D}$ at t_o. The (+) corresponds to "left hand screw" RV rotational sense, while (-) applies to "right hand screw" RV rotational sense. Δ is the

IA-61,675

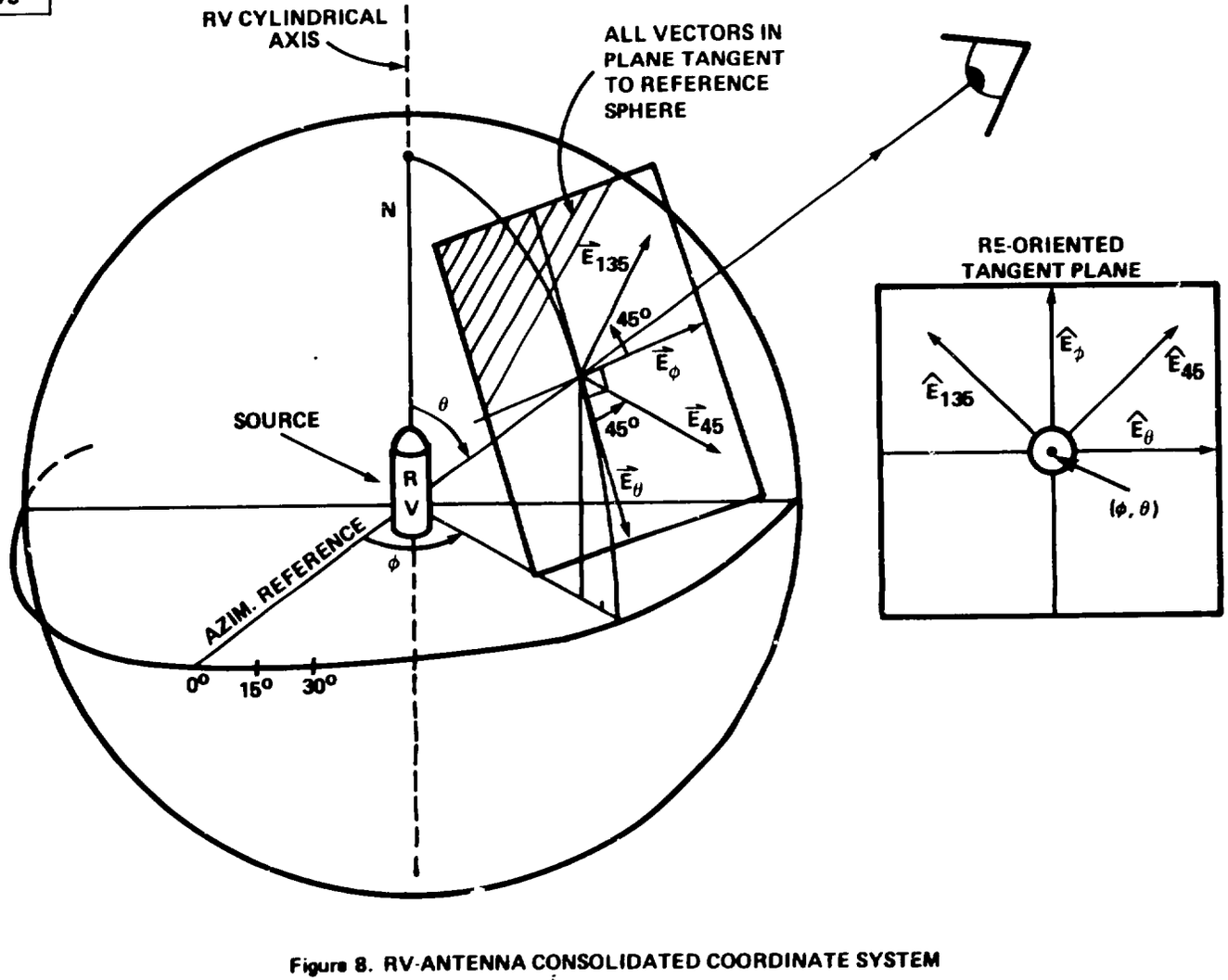

Figure 8. RV-ANTENNA CONSOLIDATED COORDINATE SYSTEM

IA-61,896

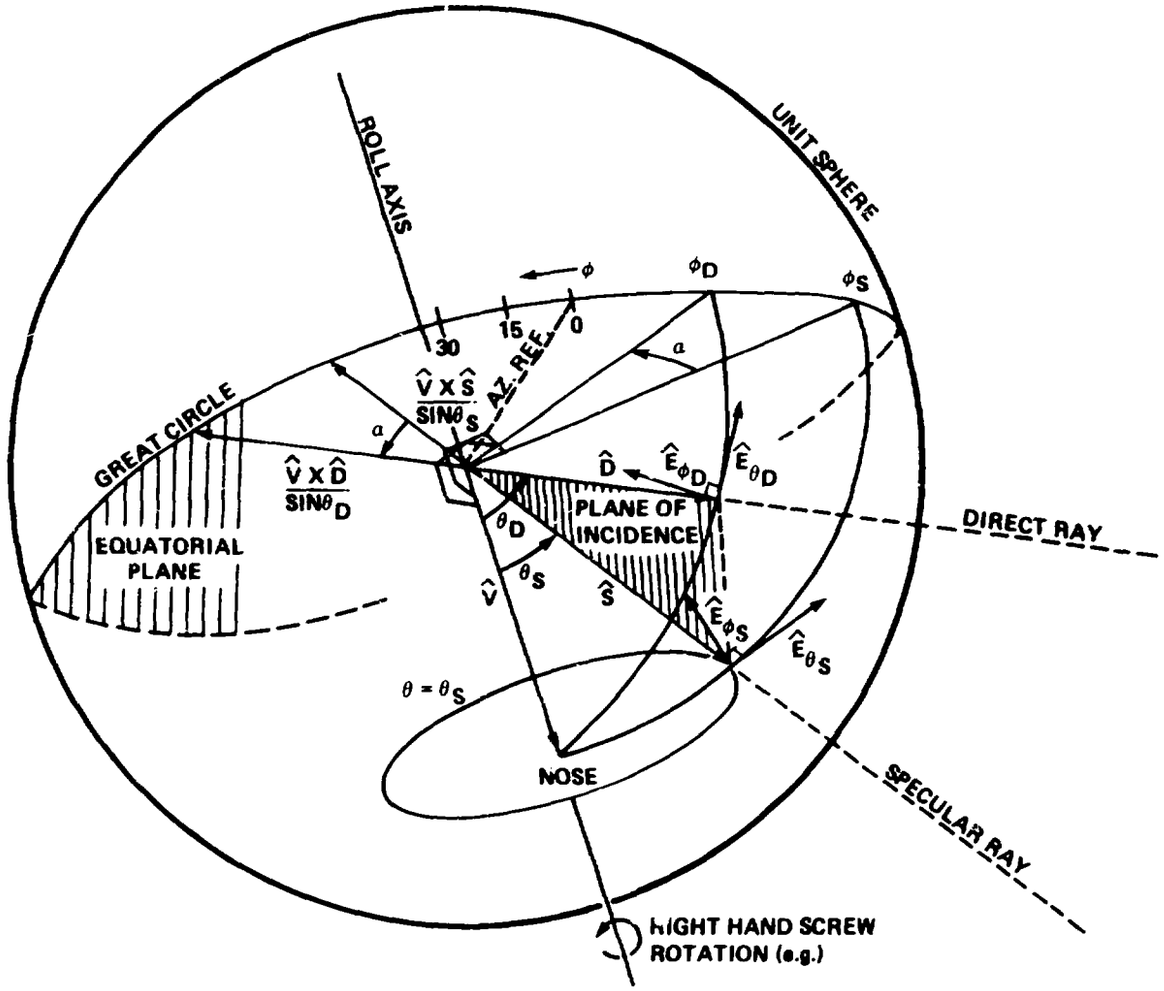

Figure 9. DIRECT AND SPECULAR RAYS REFERENCED TO RVCCS

separation in azimuth of the $\hat{D}$ and $\hat{S}$ unit vectors and has a magnitude given by*,

$$|\Delta| = \cos^{-1}\left[\frac{\hat{V} \times \hat{D} \cdot \hat{V} \times \hat{S}}{\sin\theta_S \sin\theta_D}\right] \tag{44}$$

and sign given by,

$$\text{SIGN}(\Delta) = \text{SIGN}\,[(\hat{V} \times \hat{S}) \times (\hat{V} \times \hat{D}) \cdot \hat{V}] \tag{45}$$

The preceding equations specify the directions in RVCCS of the direct and specular path rays as a function of RV position and velocity. Values of the RV antenna field amplitudes (gains), and the phase angle separating them, corresponding to these directions can be stored in a computer memory following derivation using experimental measurements.

The linear polarization unit vectors $\hat{E}_\theta$ and $\hat{E}_\phi$ are illustrated in Figure 8. The $\hat{E}_\phi$ direction is generated by the tip of the coordinate vector when infinitesmally incrementing ϕ with θ constant. Similarly, the $\hat{E}_\theta$ direction is generated by the tip of the coordinate vector when θ is infinitesmally incremented with ϕ held constant. Thus, $\hat{E}_\theta$ and $\hat{E}_\phi$ are orthogonal and tangent to the reference sphere as illustrated in Figure 8.

Since the experimentally determined field amplitudes E_θ and E_ϕ are specified in the RVCCS, it is necessary to perform a transformation to obtain the horizontal and vertical components, E_H

* See Appendix A.

and E_V. The vertical polarization lies in the plane of incidence while the horizontal polarization direction is perpendicular to the plane of incidence. To determine the transformation angles, the horizontal polarization direction, which is the same for both the specular and direct fields, must be identified. Since both $\vec{D}$ and $\vec{S}$ lie in the plane of incidence, a unit vector in the horizontal polarization direction, $\hat{H}$, is easily constructed:

$$\hat{H} = \frac{\vec{S} \times \vec{D}}{|\vec{S} \times \vec{D}|} \tag{46}$$

Since $\vec{E}_{\phi}$ is perpendicular to the azimuth plane in RVCCS designated by ϕ, $\vec{E}_{\phi D}$ is parallel to $\hat{V} \times \hat{D}$ and $\vec{E}_{\phi S}$ is parallel to $\hat{V} \times \hat{S}$. The required coordinate system transformation angles can be obtained by determining the angles (including sign of the angle) between $\hat{V} \times \hat{D}$ and $\hat{H}$ and $\hat{V} \times \hat{S}$ and $\hat{H}$ as illustrated in Figure 10.

$$|\eta_D| = \cos^{-1}\left[\frac{\hat{V} \times \hat{D} \cdot \hat{H}}{\sin \theta_D}\right] \tag{47a}$$

$$\text{SIGN}\ (\eta_D) = \text{SIGN}\left[(\hat{V} \times \hat{D}) \times \hat{H} \cdot \hat{D}\right] \tag{47b}$$

$$|\eta_S| = \cos^{-1}\left[\frac{\hat{V} \times \hat{S} \cdot \hat{H}}{\sin \theta_S}\right] \tag{48a}$$

$$\text{SIGN}\ (\eta_S) = \text{SIGN}\left[(\hat{V} \times \hat{S}) \times \hat{H} \cdot \hat{S}\right] \tag{48b}$$

A sinusoidal electric field of general polarization may be expressed (for the direct field) in terms of two linear polarization components and the phase angle between them:

$$\vec{V}_{\phi D}(t) = V_{\phi D} \cos\ (\omega t)\ \hat{V}_{\phi D} \tag{49}$$

$$\vec{V}_{\theta D}(t) = V_{\theta D} \cos\ (\omega t - \delta_D)\ \hat{V}_{\theta D} \tag{50}$$

IA-62,009

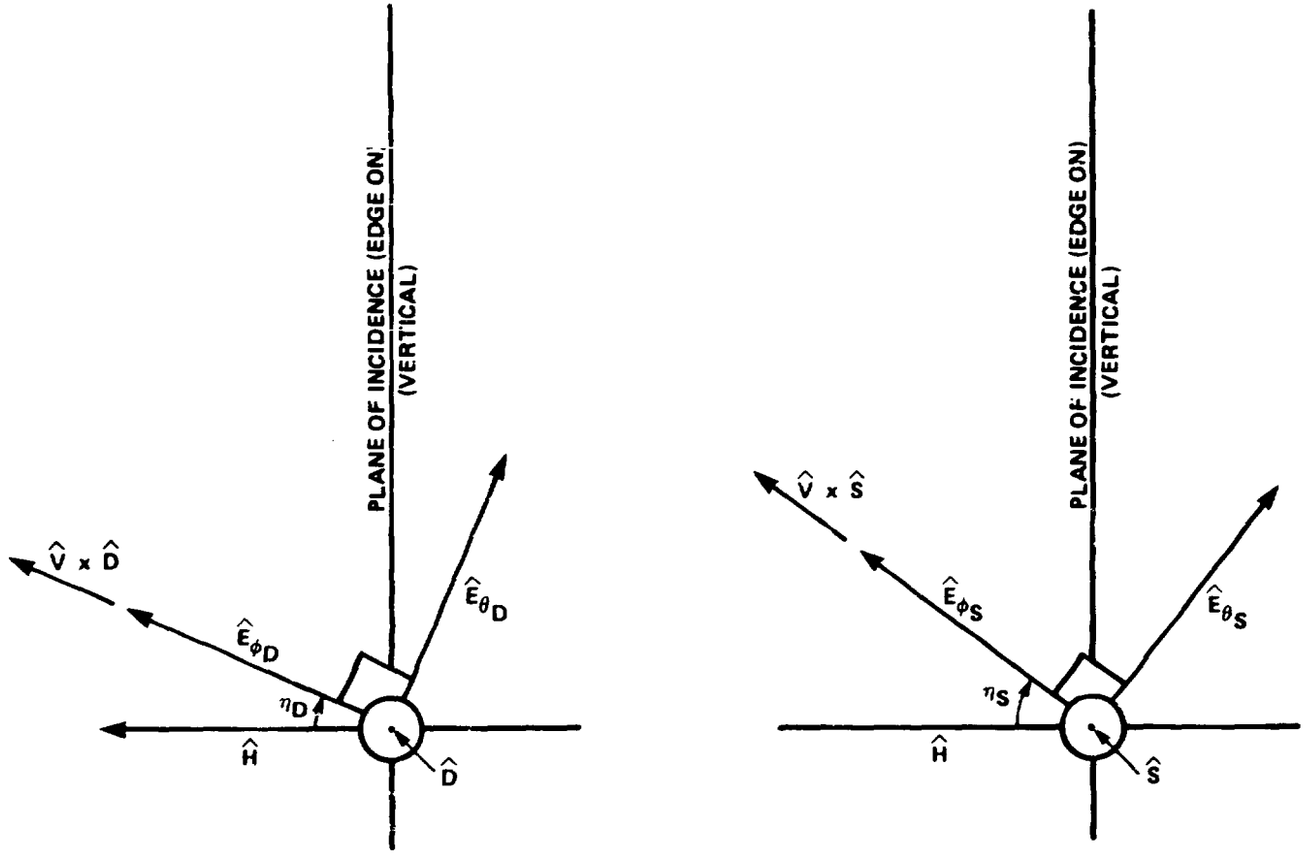

Figure 10. ILLUSTRATION OF TRANSFORMATION TO HORIZONTAL COORDINATE SYSTEM

If $\delta_D = 0, \pi, -\pi$ the resultant field is linear. If $0 < \delta_D < \pi$ the field is elliptical with a left handed rotational sense, while if $-\pi < \delta_D < 0$, the field is right-handed elliptical. Thus, the sense information is contained in the sign of δ_D.

The transformation to vertical and horizontal polarization components is given by:

$$\vec{V}_D^H(t) = [V_{\phi D}\cos(\omega t)\cos\eta_D - V_{\theta D}\cos(\omega t-\delta_D)\sin\eta_D]\,\hat{H} \tag{51}$$

$$\vec{V}_D^V(t) = [V_{\phi D}\cos(\omega t)\sin\eta_D + V_{\theta D}\cos(\omega t-\delta_D)\cos\eta_D]\,\hat{V}_D^V \tag{52}$$

These equations may be re-expressed to display the amplitudes and phases explicitly,

$$\vec{V}_D^H(t) = V_D^H \cos\left[\omega t + \mathrm{TAN}^{-1}\left(\frac{V_{\theta D}\ \mathrm{SIN}\ \eta_D\ \mathrm{SIN}\ \delta_D}{V_{\phi D}\ \mathrm{COS}\ \eta_D - V_{\theta D}\ \mathrm{SIN}\ \eta_D\ \mathrm{COS}\ \delta_D}\right)\right]\hat{H} \tag{53}$$

$$\vec{V}_D^V(t) = V_D^V \cos\left[\omega t - \mathrm{TAN}^{-1}\left(\frac{V_{\theta D}\ \mathrm{COS}\ \eta_D\ \mathrm{SIN}\ \delta_D}{V_{\phi D}\ \mathrm{SIN}\eta_D + V_{\theta D}\ \mathrm{COS}\eta_D\ \mathrm{COS}\delta_D}\right)\right]\hat{V}_D^V \tag{54}$$

in which,

$$V_D^H = [V_{\phi D}^2\cos^2\eta_D + V_{\theta D}^2\sin^2\eta_D - 2V_{\phi D}V_{\theta D}\cos\eta_D\sin\eta_D\cos\delta_D]^{1/2} \tag{55}$$

$$V_D^V = [V_{\phi D}^2\sin^2\eta_D + V_{\theta D}^2\cos^2\eta_D + 2V_{\phi D}V_{\theta D}\cos\eta_D\sin\eta_D\cos\delta_D]^{1/2} \tag{56}$$

The corresponding expressions for the specular field are obtained by replacing subscripts "D" with subscripts "S". For example, the specular component amplitudes are:

$$V_S^H = [V_{\phi S}^2 \cos^2 \eta_S + V_{\theta S}^2 \sin^2 \eta_S - 2V_{\phi S} V_{\theta S} \cos \eta_S \sin \eta_S \cos \delta_S]^{1/2} \quad (57)$$

$$V_S^V = [V_{\phi_S}^2 \sin^2 \eta_S + V_{\theta_S}^2 \cos^2 \eta_S + 2V_{\phi_S} V_{\theta_S} \cos \eta_S \sin \eta_S \cos \delta_S]^{1/2} \quad (58)$$

The RV antenna pattern is introduced into the multipath fade calculation by using the experimental values of V_ϕ, V_θ and δ in the amplitude equations above. On the other hand, the relative antenna gain of the ARIA phased array can be approximated analytically.

The direct and specular rays, referenced to the APATS array antenna, are illustrated in Figure 11. For the sake of simplicity, it has been assumed that the array boresight and longitudinal axes are horizontal. Since the array longitudinal axis is parallel to the ARIA centerline, the latter assumption presupposes that the aircraft is in level flight during telemetry acquisition.

In the array coordinate system, illustrated in Figure 11, both the direct and specular rays, which lie in a vertical plane of incidence, have the same azimuth value, α. The direct ray has an elevation angle γ, which is the RV elevation angle, while the specular ray is depressed below the horizontal, in the plane of incidence, by θ, the specular angle.

If the array elements are arranged in M rows of length A and N columns of length B, then the antenna gain in the specular direction, relative to the line of sight direction, assuming that the array is electronically steered for optimum gain along the direct path, is*,

---

* See Appendix B.

IA-62,010

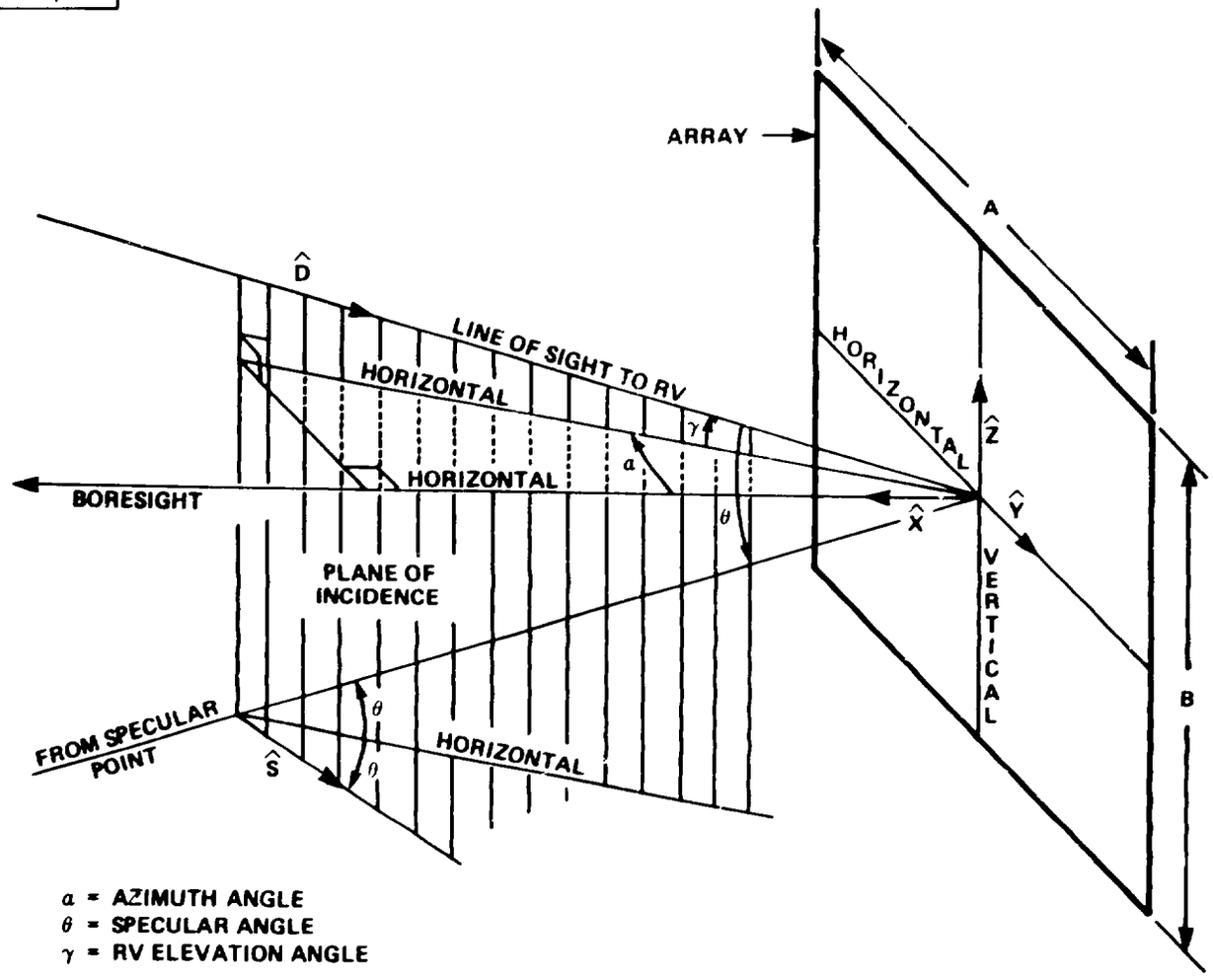

Figure 11. DIRECT AND SPECULAR RAYS REFERENCED TO RECEIVING ARRAY ANTENNA

$$g_{REL} = \frac{g(\alpha, -\theta)}{g(\alpha, \gamma)} = \frac{\mathrm{SIN}^2\left[\frac{\pi A}{\lambda}\,\mathrm{SIN}\,\alpha(\mathrm{COS}\,\theta - \mathrm{COS}\gamma)\right]}{N^2\,\mathrm{SIN}^2\left[\frac{\pi A}{N\lambda}\,\mathrm{SIN}\,\alpha(\mathrm{COS}\,\theta - \mathrm{COS}\gamma)\right]} \times$$

$$\frac{\mathrm{SIN}^2\left[\frac{\pi B}{\lambda}\,(\mathrm{SIN}\,\theta + \mathrm{SIN}\gamma)\right]}{M^2\,\mathrm{SIN}^2\left[\frac{\pi B}{M\lambda}\,(\mathrm{SIN}\,\theta + \mathrm{SIN}\gamma)\right]}\left(\frac{\mathrm{COS}\,\theta}{\mathrm{COS}\gamma}\right) \tag{59}$$

If the array elements are separated by $\lambda/2$ and the direct and specular rays are not widely separated, i.e., if,

$$\frac{\pi}{2}\,[\mathrm{SIN}\,\alpha(\mathrm{COS}\,\theta - \mathrm{COS}\,\gamma)] \ll 1 \tag{60a}$$

and,

$$\frac{\pi}{2}\,(\mathrm{SIN}\,\theta + \mathrm{SIN}\,\gamma) \ll 1 \tag{60b}$$

Then equation (59) may be replaced by the approximation,

$$g_{REL} = \frac{\mathrm{SIN}^2\left[\frac{\pi A}{\lambda}\,\mathrm{SIN}\,\alpha(\mathrm{COS}\theta - \mathrm{COS}\gamma)\right]\,\mathrm{SIN}^2\left[\frac{\pi B}{\lambda}(\mathrm{SIN}\theta + \mathrm{SIN}\gamma)\right]}{\left[\frac{\pi A}{\lambda}\,\mathrm{SIN}\alpha(\mathrm{COS}\theta - \mathrm{COS}\gamma)\right]^2\left[\frac{\pi B}{\lambda}\,(\mathrm{SIN}\theta + \mathrm{SIN}\gamma)\right]^2\left(\frac{\mathrm{COS}\,\gamma}{\mathrm{COS}\,\theta}\right)} \tag{61}$$

and the relative voltage amplitude at the array output associated with the direct and specular fields is given by the square root of g_{REL}.

The space loss of the specular path field relative to the direct path field is designated R_{SL}.

All the major factors necessary to evaluate the depth of the RF power fade have now been considered. The maximum depth of fade occurs when the amplitudes of the direct and specular fields are in phase opposition, and in general will be different for vertical and

horizontal polarization. The net amplitude is referenced to the direct amplitude alone and therefore zero dB fade corresponds to no multipath interference. Thus, for horizontal polarization if,

$$V_D^H > \alpha_R^H \; \alpha_{SS} \sqrt{g_{REL} \; R_{SL}} \; V_S^H$$

the maximum depth of the power fade is,

$$-20 \log \left[\frac{V_D^H - \alpha_R^H \alpha_{SS} \sqrt{g_{REL} \; R_{SL}} \; V_S^H}{V_D^H} \right] \text{(dB)} \tag{62}$$

or if,

$$V_D^H < \alpha_R^H \; \alpha_{SS} \sqrt{g_{REL} \; R_{SL}} \; V_S^H$$

$$-20 \log \left[\frac{\alpha_R^H \alpha_{SS} \sqrt{g_{REL} \; R_{SL}} \; V_S^H - V_D^H}{V_D^H} \right] \text{(dB)} \tag{63}$$

is applicable. For vertical polarization, if,

$$V_D^V > \alpha_R^V \; \alpha_{SS} \; \sqrt{g_{REL} \; R_{SL}} \; V_S^V$$

the maximum depth of fade is,

$$-20 \log \left[\frac{V_D^V - \alpha_R^V \alpha_{SS} \sqrt{g_{REL} \; R_{SL}} \; V_S^V}{V_D^V} \right] \text{(dB)} \tag{64}$$

and if,

$$V_D^V < \alpha_R^V \alpha_{SS} \; \sqrt{g_{REL} \; R_{SL}} \; V_S^V$$

the power fade is,

$$-20 \log \left[\frac{\alpha_R^V \alpha_{SS} \sqrt{g_{REL} \; R_{SL}} \; V_S^V - V_D^V}{V_D^V} \right] \text{(dB)} \tag{65}$$

In the above, V_D^H , V_S^H , V_D^V and V_S^V are given by Eqs. (55), (56), (57), and (58) respectively.

As discussed in the previous section, fading occurs (for pure carrier interference) with a beat frequency given by the differential Doppler shift: from Equations (4c) and (4d),

$$\omega_o(D_S - D_D) = \frac{\omega_o|\vec{V}|}{C}[\hat{V} \cdot \hat{S} - \hat{V} \cdot \hat{D}]$$

$$= \frac{\omega_o|\vec{V}|}{C}(\cos\theta_S - \cos\theta_D) \qquad (66)$$

in which Equations (40) and (41) have been used.

SECTION 4

CALCULATIONS

In the previous section, the factors required to calculate the depth of RF fading and frequency of fade for the basic multipath model were discussed in detail. Here the results of calculations are presented and used to illustrate and support some of the conclusions which were advanced in Section 1.

The results of purely geometrical calculations of the relative channel time delay are illustrated in Figure 12. The flat earth approximation was used in these computations so that the delays are slightly exaggerated relative to those which would have been obtained from a rigorous curved earth calculation. The delay increases linearly with ARIA altitude for a given baseline and RV height. If 10% intersymbol interference is deemed tolerable,[1] a symbol rate of up to 65 k/s is feasible if the ARIA is at 9 km and RV is at 1 km, for example.

In Figure 13 the differential Doppler shift as a function of ARIA altitude is plotted for three different RV trajectories. Trajectory A is predominantly vertical and yields a large Doppler shift. Trajectory C is mainly transverse and therefore shows relatively weak Doppler shifts, while trajectory B represents an "average" situation in which the magnitudes of all velocity components are equal. In each case, however, the difference between the Doppler shifted frequencies increases nearly linearly with ARIA altitude for a given RV height and baseline. As noted previously, Doppler shifts can be particularly troublesome vis-a-vis subcarrier interference and modulation distortion--a topic which requires further in-depth study.

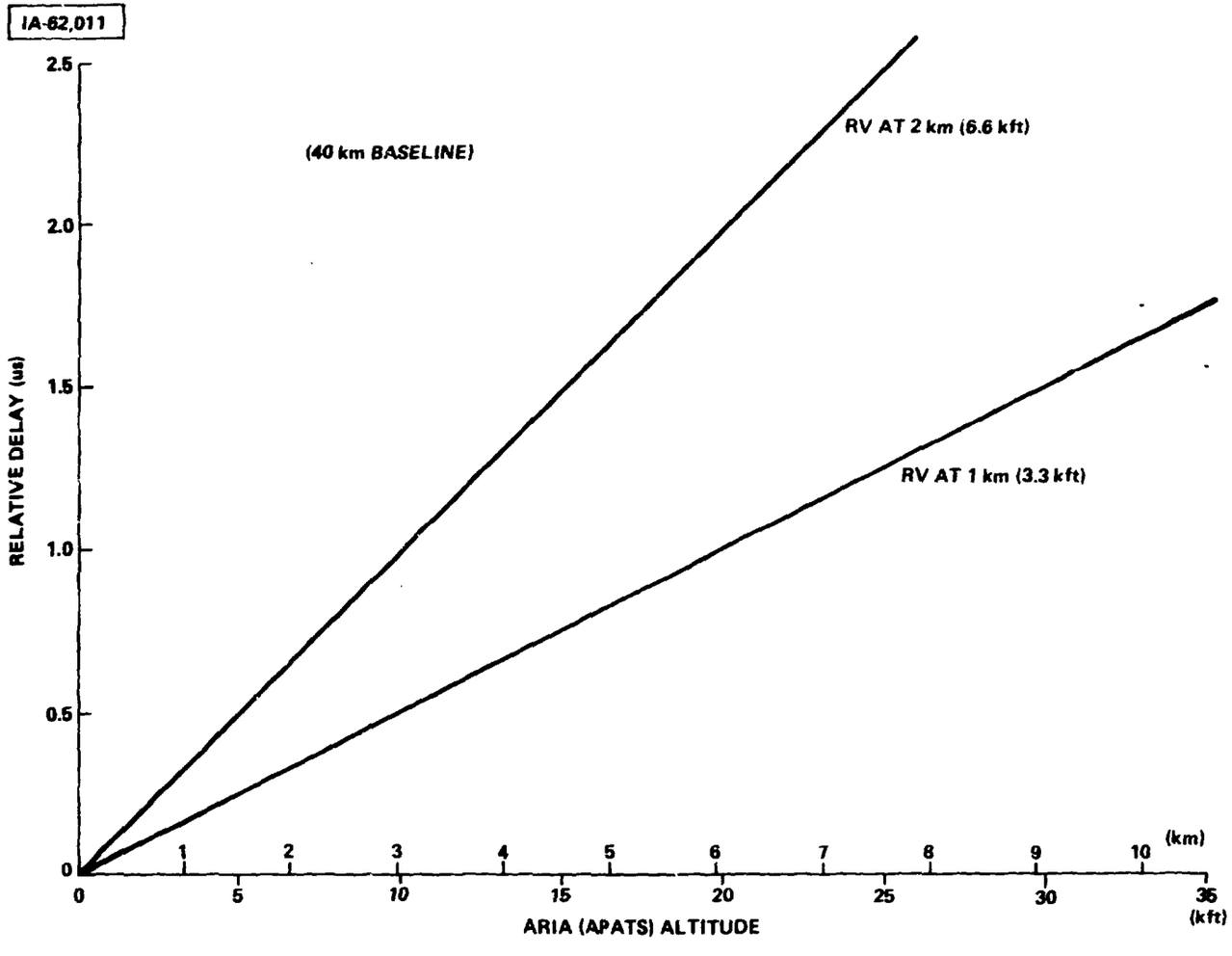

Figure 12. TIME DELAY DIFFERENCE VS. ARIA ALTITUDE

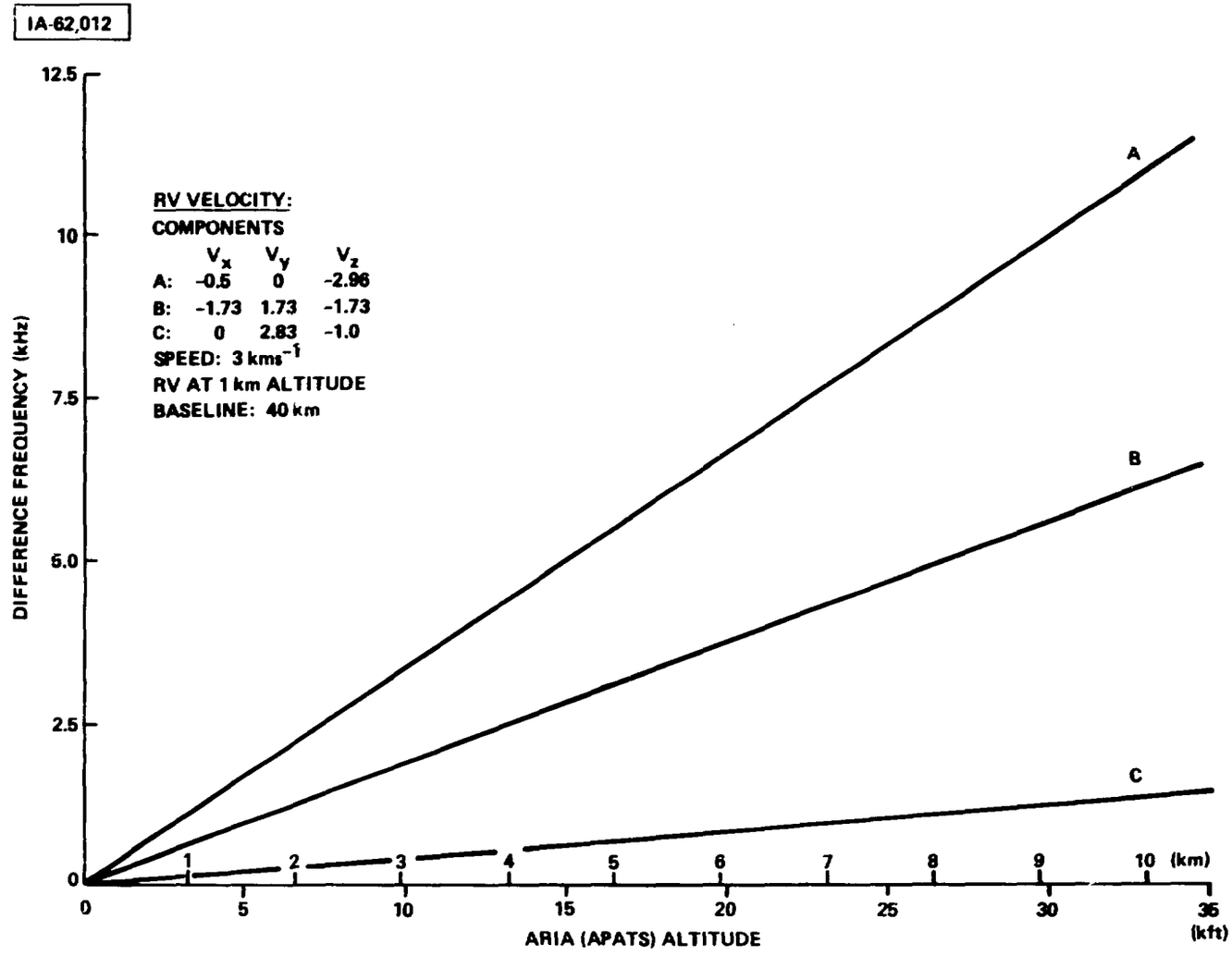

Figure 13. DIFFERENTIAL DOPPLER SHIFT VS. ARIA ALTITUDE

To calculate RF power fades, the RV antenna radiation pattern is required if truly realistic results are to be obtained, however, in lieu of an actual experimental pattern, which had not yet been interfaced with the computer at the time of this writing, a "dummy" pattern was used. The pattern so employed is that of a dipole parallel to the RV axis with a deeply scalloped azimuthal dependence intended to crudely imitate nulls (~25 dBi) in the true antenna pattern. More specifically,

$$V_\theta \propto \sin\theta[0.05 + 0.95|\cos\phi|^{1/2}];\ V_\phi = 0 \qquad (67)$$

were employed. The model gain is displayed in Figure 14 for $\theta = 90^\circ$. For all calculations the RV was assumed to roll at $720^\circ\ s^{-1}$. The local coordinate system shown in Figure 15 was employed throughout these calculations for simplicity. All of these calculations were performed using an HP41C programmable calculator system.

In Figures 16 and 17 the calculated maximum RF fade depths for horizontal polarization, as referenced to the direct signal strength, are plotted as a function of RV altitude for an ARIA altitude of 2 km. For the case illustrated by Figure 16, the RV velocity, which is assumed to be constant for the altitude range considered, is predominantly vertical, while for Figure 17 the trajectory is predominantly horizontal. Since computations of the fade depth were performed at 10 m intervals of altitude, areas of the plot for which the fade is varying rapidly are either indicated with dashed lines or point values. Points marked by a cross specify fades for which the specular voltage exceeds the direct voltage at the array output.

Two strong features of these theoretical curves are immediately evident: (1) on the average, the fades become gradually deeper as

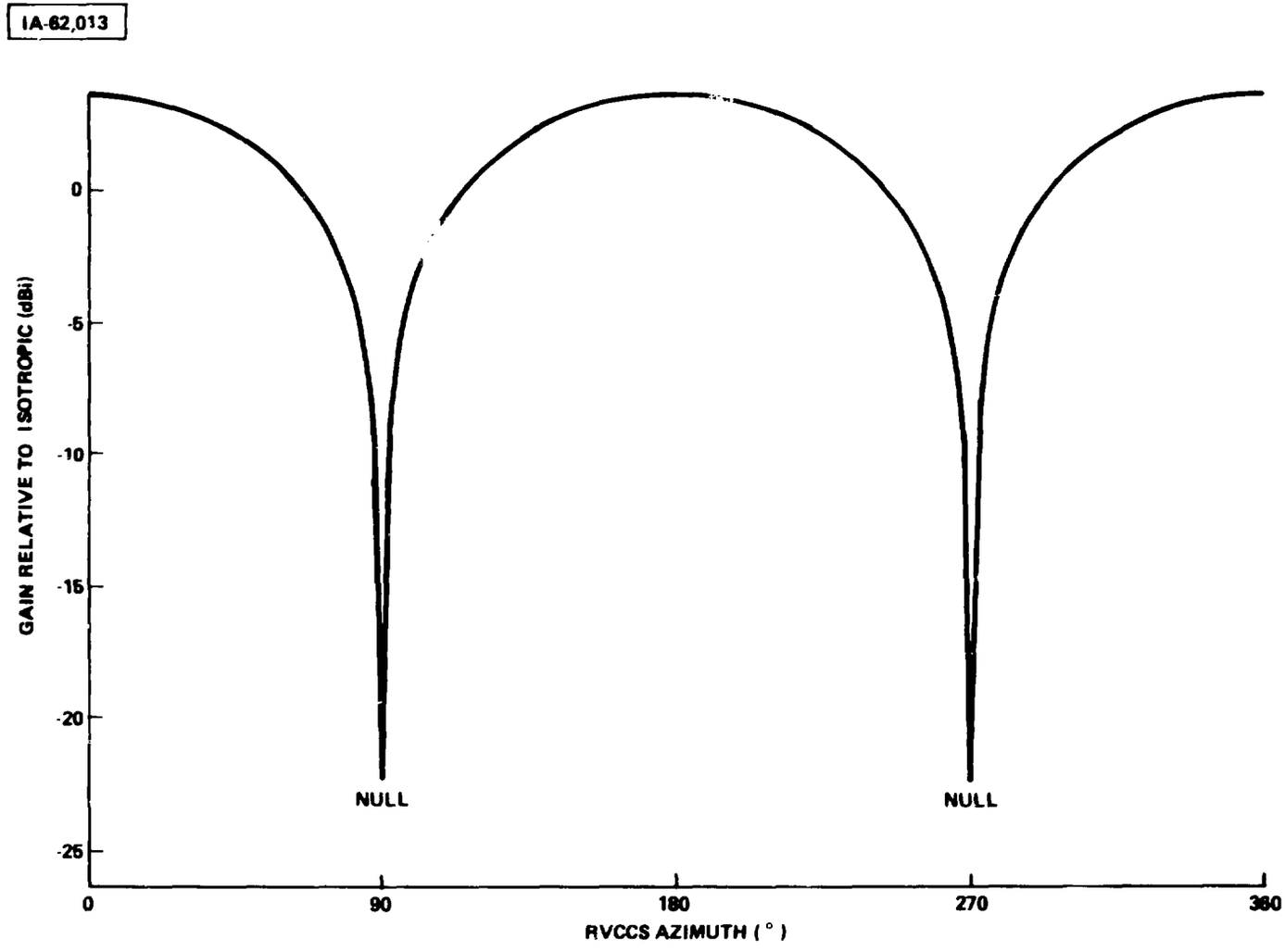

Figure 14. MODEL RV ANTENNA GAIN FUNCTION

IA-62 014

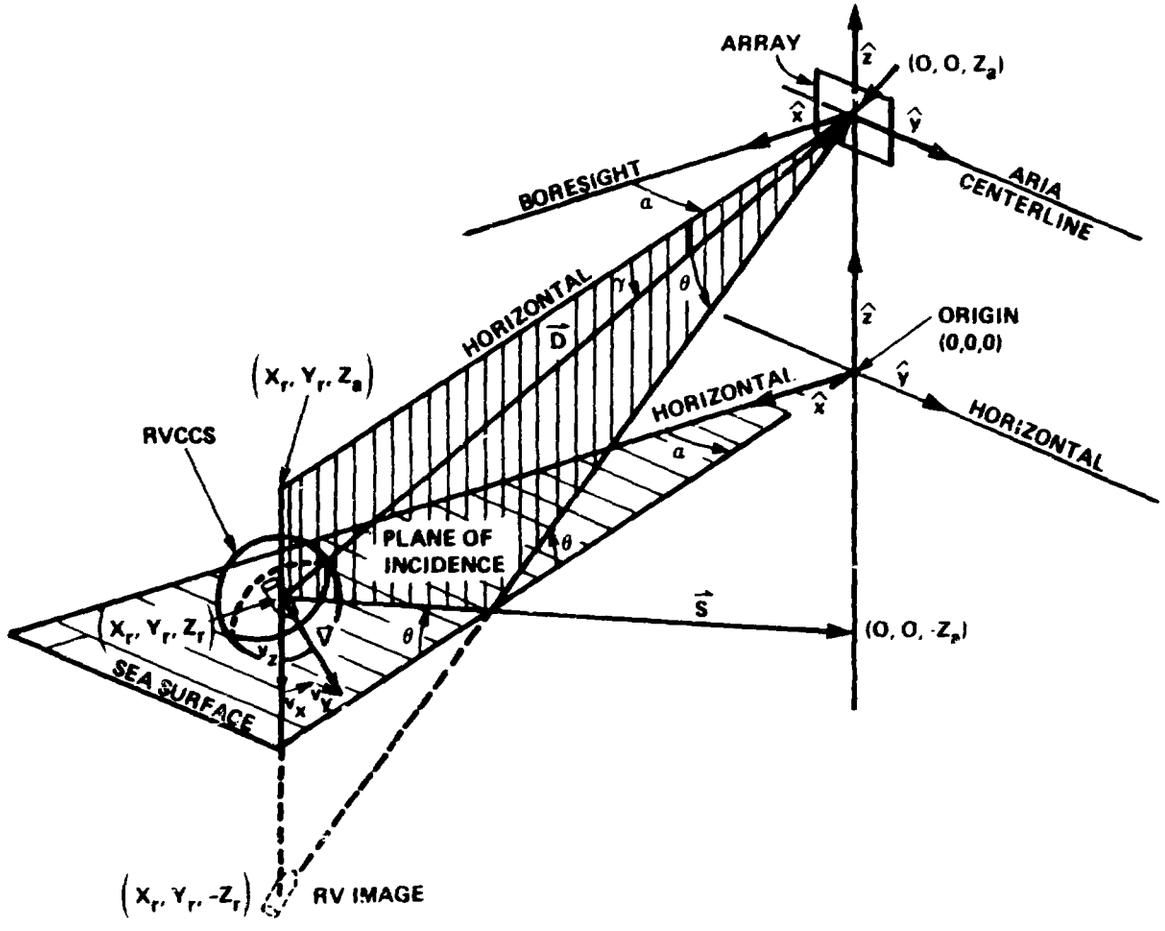

Figure 15. SIMPLIFIED LOCAL COORDINATE SYSTEM

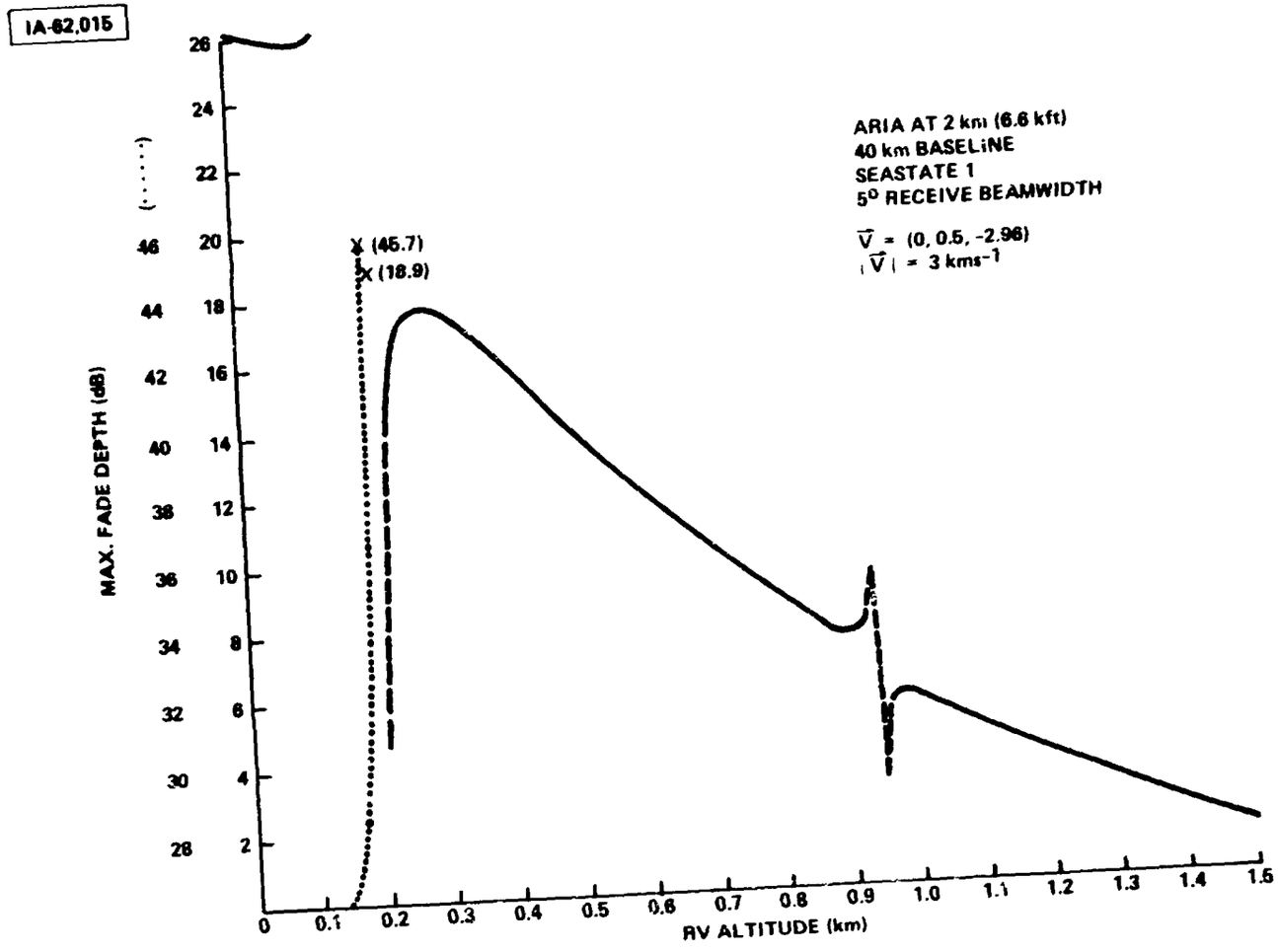

Figure 16. RF FADE FOR NEARLY VERTICAL RV TRAJECTORY

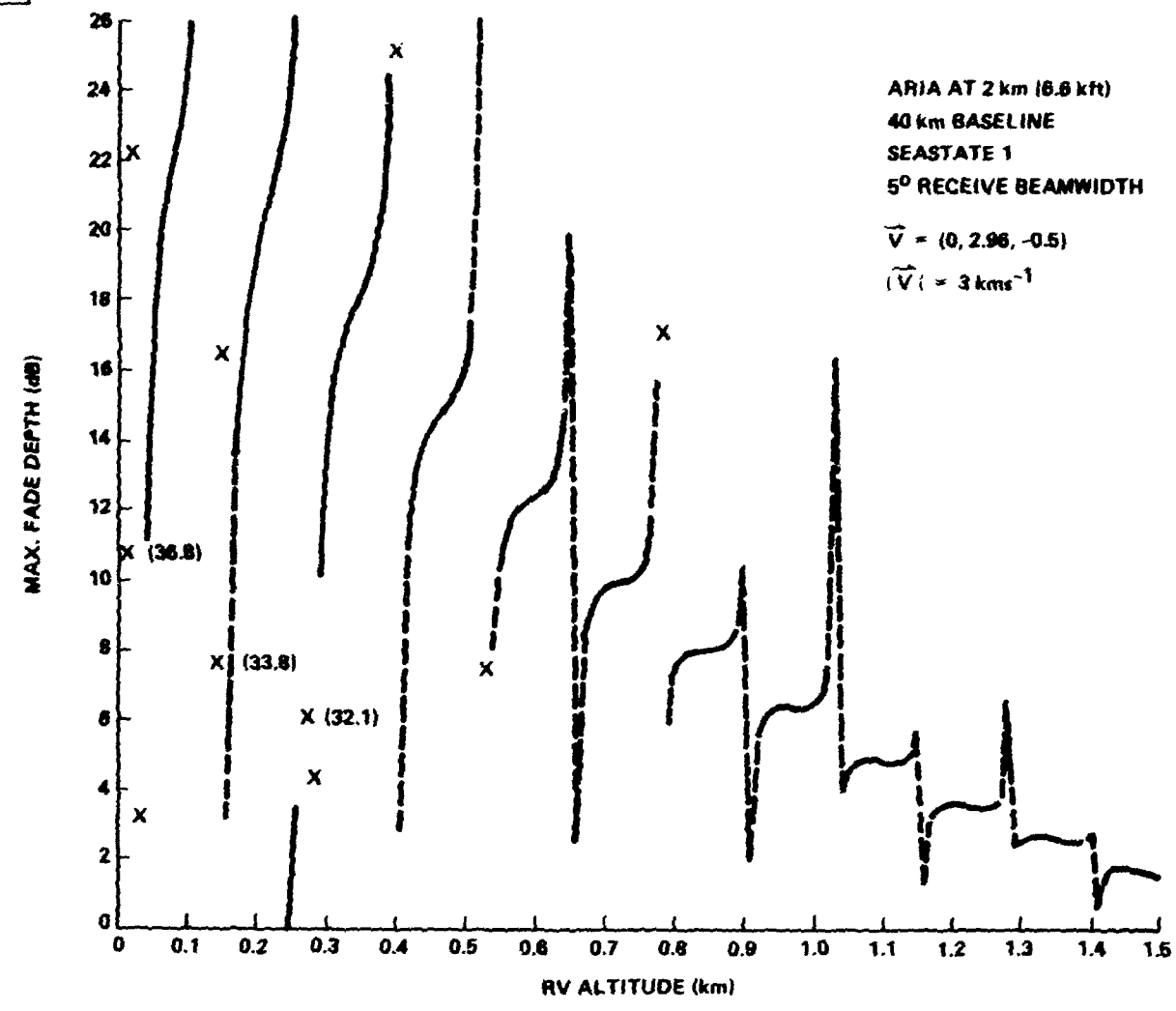

Figure 17. RF FADE FOR NEARLY HORIZONTAL RV TRAJECTORY

the RV descends, and (2) the curves are "modulated" by large spikes which occur at intervals which correspond to the vertical distance through which the RV moves in the time required for it to execute a rotation of 180°. Closer examination of these results reveals that feature (1) is a consequence of the relative ARIA antenna gain for the direct and specular beam, while feature (2) results from the interplay of the RV antenna pattern, RV rotation, and the specular multipath geometry. More specifically, when the RV velocity vector does not lie in the plane of incidence of the specular beam, the direct and specular rays have different azimuth values in the RV-Antenna Consolidated Coordinate System (RVCCS). When a null in the model antenna pattern rotates through the plane of incidence, the relative strengths of the direct and specular beams alternate. In the examples illustrated in Figures 16, 17 and those that follow, the RV rotation is such that the specular direction intercepts the antenna null before the direct direction, hence fades are alleviated initially, but become much worse when the direct beam direction aligns with the null several degrees or so of RV rotation later. The peak-to-peak spike deflection is a function of the antenna null depth and the azimuthal separation of the direct and specular rays in the RVCCS. This azimuthal separation is a function of RV trajectory and RV-ARIA geometry and is given by Eq. 45. Generally, the azimuthal separation angle, Δ, is larger for lower RV penetration angles and for a given RV trajectory increases as the ARIA altitude increases, as shown in Appendix A, Figure 23.

Thus, nulls in the RV antenna pattern (or any large antenna power variations occurring over angles the order of the azimuth separation angle) can lead to brief but extremely deep RF power fades relative to those which might be anticipated for an isotropic transmitter. In addition, these multipath fades will occur at times when the direct signal strength is already low. The frequency of

the deep fades, in the context of the present model, is twice the RV rotational frequency, since two nulls are intercepted for every rotation of the RV. If the RV trajectory is nearly horizontal, as is the case in Figure 17, more deep fades can be witnessed since the RV is aloft longer than would be the case for a vertical trajectory, assuming RV speed is constant.

Figures 18, 19 and 20 illustrate the dependence of fade depth on ARIA altitude. A smooth sea surface (sea state 1, σ_h = 6.5 cm) is assumed to realistically model the worst multipath environment likely to be encountered in the broad ocean area. For all RV and ARIA altitudes, horizontal polarization suffers far deeper fades than vertical polarization. This result follows from the behavior of the Fresnel reflection coefficients. In particular, for sea water, the amplitude of the vertical polarization Fresnel coefficient has a minimum of 0.1 at 6° grazing incidence (Brewster angle). The near absence of vertical polarization multipath fading near this angle is evident for the RV-ARIA geometry of Figure 19, since the ARIA altitude of 4 km over a baseline of 40 km yields a specular grazing angle of about 6°. The amplitude of the horizontal polarization Fresnel coefficient is nearly unity for grazing angles less than 20°, so that the fades are generally reduced only by sea roughness and the receiving antenna directivity. In this connection it is evident, that for a given sea state, a larger specular grazing angle, as is subtended by a higher flying ARIA, will reduce fading, at least in the context of the coherent specular multipath model, and an isotropic RV antenna power pattern.

Figure 21 illustrates the influence of ocean surface roughness on RF multipath fading for a nominal trajectory. It is realized that for a non-smooth sea diffuse or incoherent multipath must be considered; however, the present model, which neglects incoherent

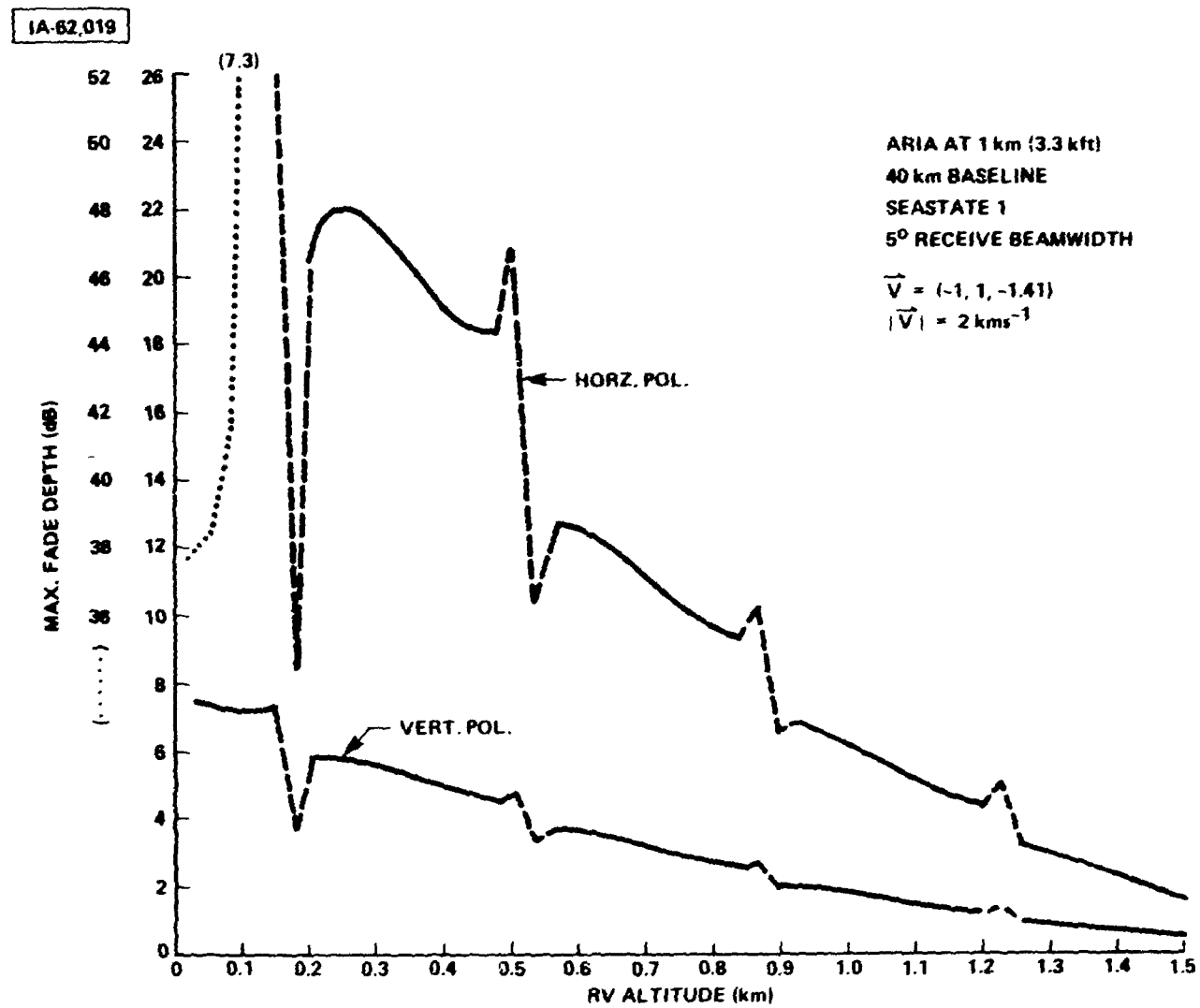

Figure 18. RF FADE FOR ARIA AT 1 km ALTITUDE

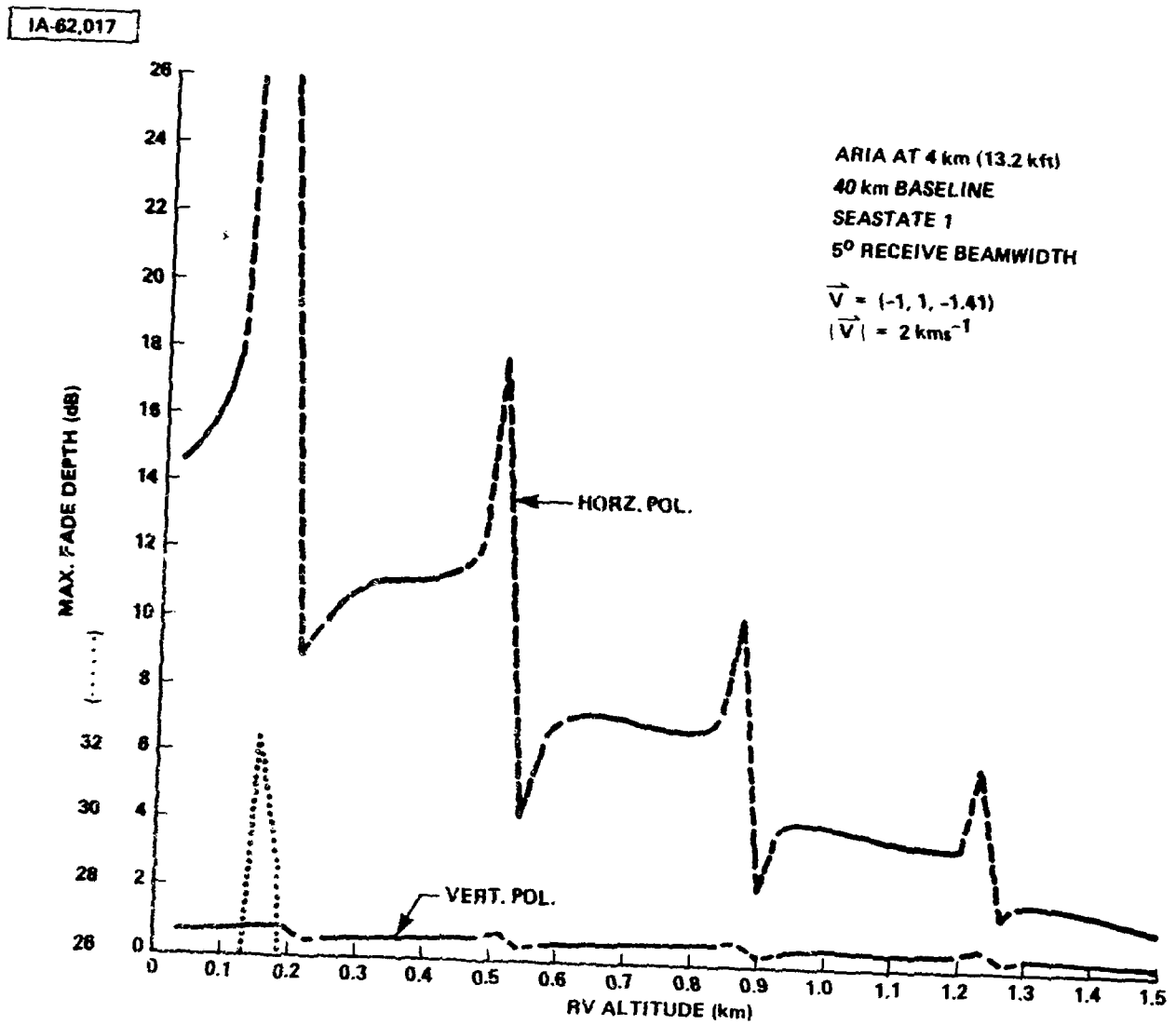

Figure 19. RF FADE FOR ARIA AT 4 km ALTITUDE

IA-62,018

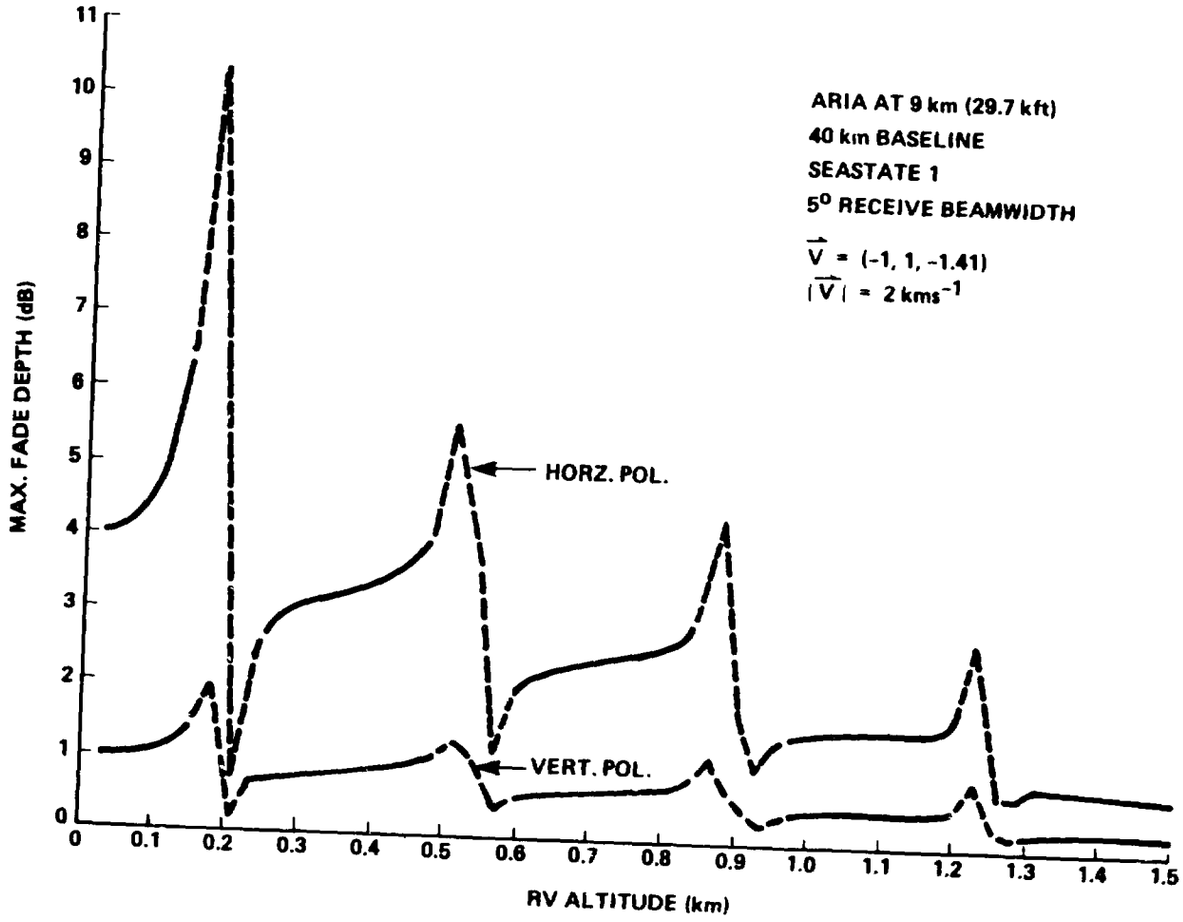

Figure 20. RF FADE FOR ARIA AT 9 km ALTITUDE

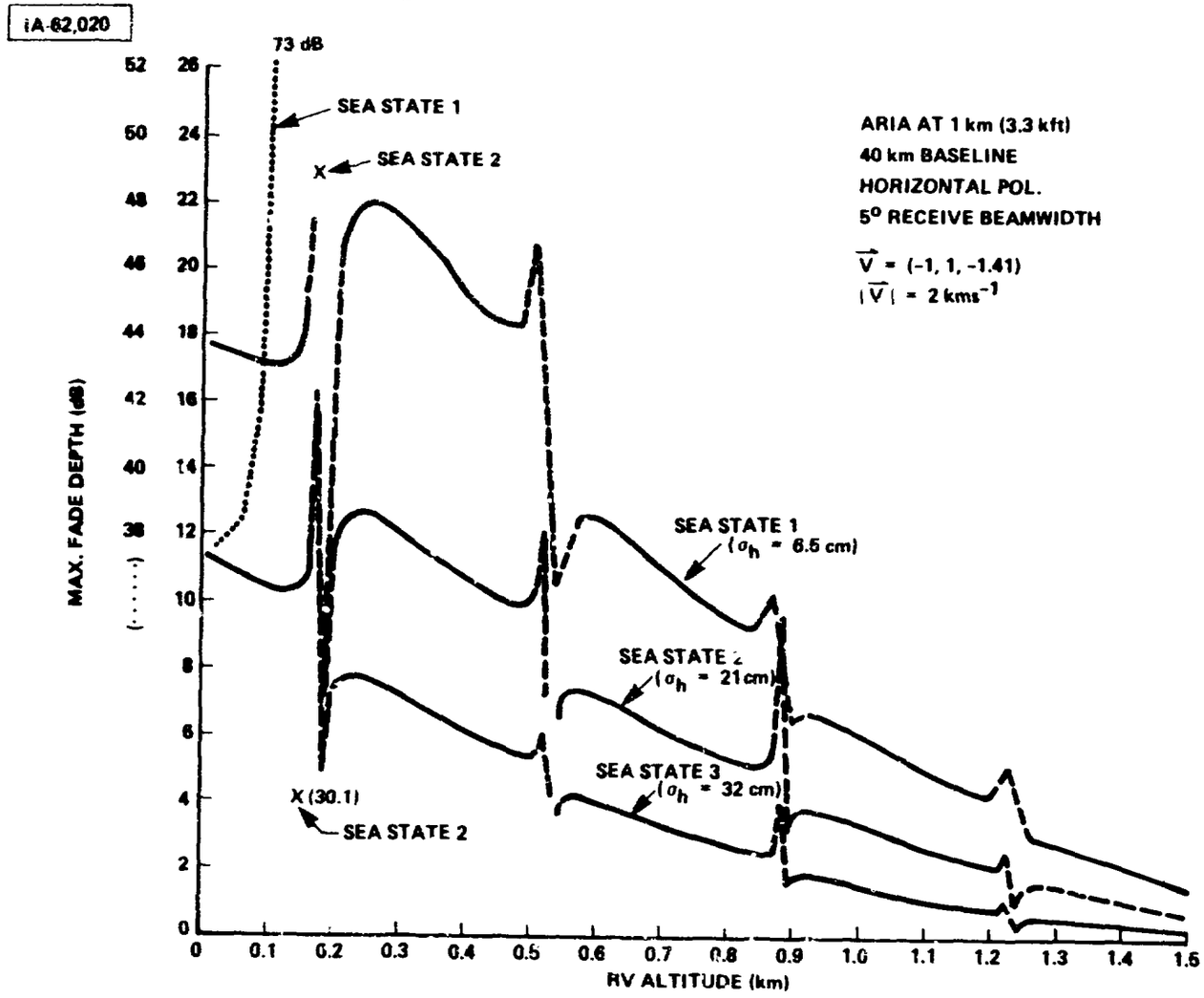

Figure 21. RF FADE VERSUS SEA STATE

scatter, indicates that significantly better system performance can be expected for test support positions over rough seas.

The first conclusion in Section 1 was predicated on a 4° ARIA antenna beamwidth, which roughly corresponds to the 150 cm array vertical length used throughout the previous calculations (approx. 3 dB beamwidth $\simeq \sin^{-1}(\lambda/b)$). The subject of Figure 22 is the relationship between array length ("B" in Eq. 61) and RF fade depth, with all other parameters constant. Clearly, for the higher RV altitudes shown, the larger arrays reduce fade considerably by discriminating against the specular path beam. Approximate beamwidths are noted adjacent to the array size in the figure key. Note that for the 1.5 m array, the specular beam falls into a null at an RV altitude of 1.75 km.

In Section 1, reference was made to a study[1] which purports to show that multipath is a problem for ARIA missions at VHF with a relatively low-gain receiving antenna. The present and proposed (APATS) ARIA systems are at S-band (2.2 GHz) and incorporate high gain (~28-32 dB) receiving antennas. In principle, multipath should be greatly alleviated by both of these factors, since sea roughness is much more pronounced for shorter wavelength radiation and the specular multipath channel should be reduced. On the other hand, differential Doppler shift is much greater at S-band and can become a nuisance. In any case "multipath" still interferes with efficient telemetry detection at higher, more desirable ARIA altitudes at S-band, so further study of multipath interference is required, with emphasis on the influence of telemetry support altitude.

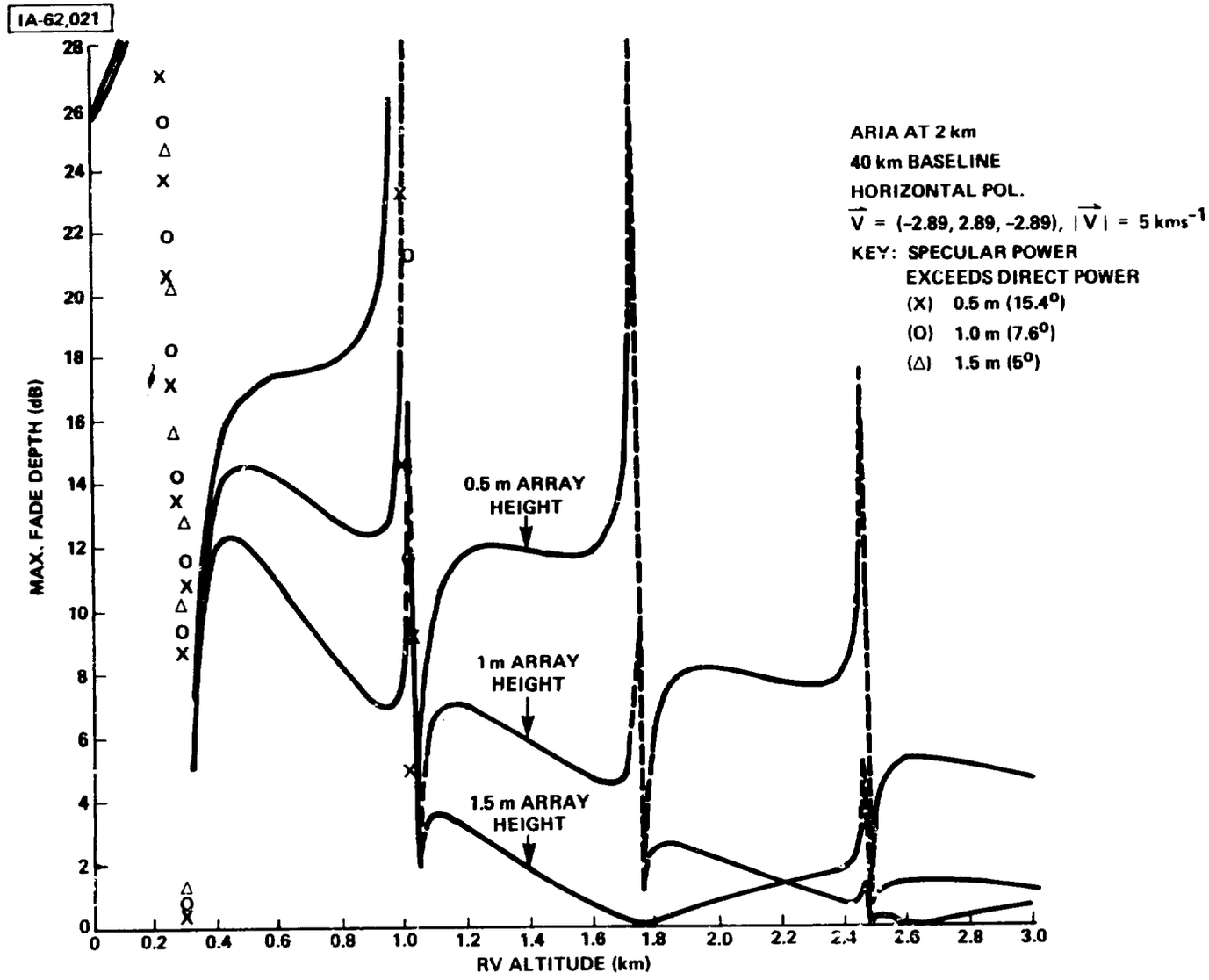

Figure 22. RF FADE VERSUS ARRAY HEIGHT (RECEIVE BEAMWIDTH)

REFERENCES

1) W. R. Hedeman and M. H. Nichols, "Multipath Constraints on Telemetry Data Transmission," Report No. TOR-0200 (S4816-88)-2, Aerospace Corporation, San Bernardino, CA, June 1969.

2) P. H. Panter, Modulation, Noise, and Spectral Analysis, (McGraw-Hill, 1965) p. 355.

3) E. J. Baghdady, "Frequency-Modulation Interference Rejection with Narrow Band Limiters," Proc. IRE, Vol. 43, Jan 1955, p. 51.

4) H. R. Reed and C. M. Russel, Ultra High Frequency Propagation, (John Wiley and Sons, New York, 1953) p. 90.

5) Ref. 5, p. 84.

6) P. Beckmann and A. Spizzichino, The Scattering of Electromagnetic Waves From Rough Surfaces, (MacMillan Co., New York, 1963) p. 246.

7) C. I. Beard, "Coherent and Incoherent Scattering of Microwaves From the Ocean," IRE Trans. AP-9, No. 5, Sept. 1961, p. 474.

8) D. K. Barton and H. R. Ward, Handbook of Radar Measurement, (Prentice-Hall, Englewood Cliffs, NJ, 1969) p. 148.

9) "IRIG Standard Coordinate System and Data Formats for Antenna Patterns," May 1966, AD637 189.

APPENDIX A

RVCCS AZIMUTH DETERMINATION

The vectors $\hat{V}$, $\hat{D}$ and $\hat{S}$ are conveniently specified in the local coordinate system illustrated in Figure 15; however, it is necessary to determine the angular coordinates (ϕ, θ) of $\hat{D}$ and $\hat{S}$ in the RV consolidated coordinate system (RVCCS) in order to determine the RV antenna gain in the direct and specular directions, respectively. Since $\hat{V}$ is coincident with the polar axis of the RVCCS, the angles included between $\hat{V}$ and $\hat{D}$, and between $\hat{V}$ and $\hat{S}$ are immediately identified as θ_D and θ_S respectively, as illustrated in Figure 9. From elementary vector algebra,

$$\theta_D = \cos^{-1} [\hat{V} \cdot \hat{D}] \tag{40}$$

$$\theta_S = \cos^{-1} [\hat{V} \cdot \hat{S}] \tag{41}$$

and these angles can range from 0° to 180°. Unit vectors* which lie in the equatorial plane of the RVCCS and are perpendicular to the azimuth plane in which $\hat{D}$ and $\hat{S}$ lie are given by, respectively,

$$\frac{\hat{V} \times \hat{D}}{\sin\theta_D} \; ; \; \frac{\hat{V} \times \hat{S}}{\sin\theta_S}$$

Both of these vectors lie in the RVCCS equatorial plane and the angle between them is identical to the azimuthal separation angle of $\hat{D}$ and $\hat{S}$. The magnitude of the difference angle is readily obtained from the dot product,

$$|\Delta| = \cos^{-1} \left[\frac{\hat{V} \times \hat{D} \cdot \hat{V} \times \hat{S}}{\sin\theta_D \, \sin\theta_S} \right] \tag{44}$$

* Actually pseudovectors.

and is plotted as a function of ARIA altitude for several RV trajectories in Figure 23.

However, the sign of Δ cannot be obtained from the dot product since,

$$\mathrm{COS}(-X) = \mathrm{COS}(X)$$

Note, however, that if the cross product of the equatorial plane vectors is taken the resulting vector is either parallel or antiparallel to $\hat{V}$, depending upon the order of the equatorial vectors. If ϕ_D is greater than ϕ_S, Δ is positive (see Equation 43) and the scalar,

$$(\hat{V} \times \hat{S}) \times (\hat{V} \times \hat{D}) \cdot \hat{V} \tag{68}$$

is positive, i.e., the cross product of the equatorial vectors, taken in the order shown in (68), is a vector parallel to $\hat{V}$, which when dotted into $\hat{V}$ must yield a positive number. Similarly, if Δ is negative, the scalar given by (68) is negative, since the vectors are antiparallel. Thus, the sign of the number given by (68) is the sign of Δ as indicated in Equation (45).

If the direction of the RV velocity does not change in the time interval $t-t_o$, the unit vectors in the direct and specular directions can be represented by,

$$\hat{D}(t) = \frac{\vec{D}(t)}{|\vec{D}(t)|} = \frac{\vec{D}_{t_o} - \hat{V}\int_{t_o}^{t} |\vec{V}(t)|\, dt}{|\vec{D}(t)|} = \frac{\vec{D}_{t_o} - a\hat{V}}{|\vec{D}_{t_o} - a\hat{V}|} \tag{69a}$$

$$\hat{S}(t) = \frac{\vec{S}(t)}{|\vec{S}(t)|} = \frac{\vec{S}_{t_o} - \hat{V}\int_{t_o}^{t} |\vec{V}(t)|\, dt}{|\vec{S}(t)|} = \frac{\vec{S}_{t_o} - a\hat{V}}{|\vec{S}_{t_o} - a\hat{V}|} \tag{69b}$$

IA – 62, 215

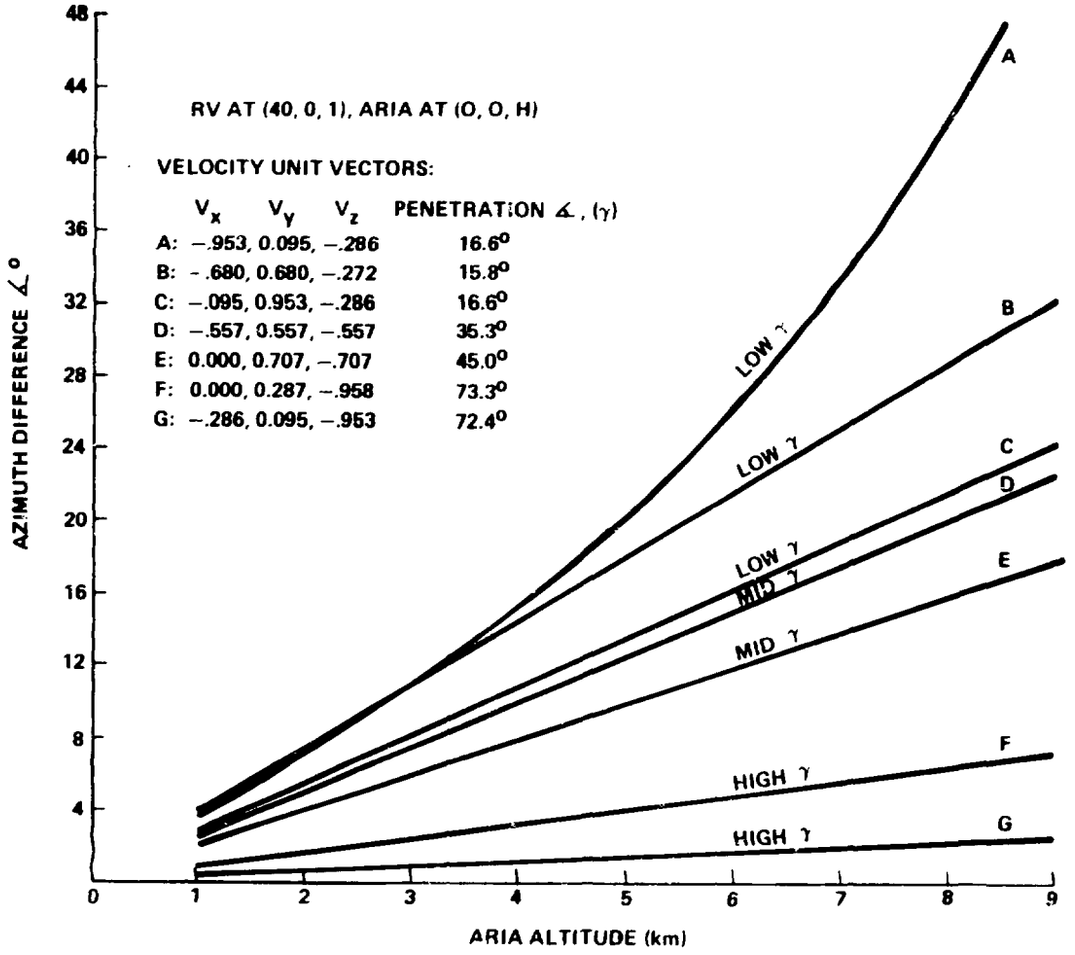

Figure 23. AZIMUTH DIFFERENCE ANGLE VERSUS ARIA ALTITUDE FOR SEVERAL RV TRAJECTORIES, A 40 km BASELINE AND RV ALTITUDE OF 1 km

$$a = \int_{t_o}^{t} |\vec{V}(t)|\, dt \tag{69c}$$

and once again the magnitude of Δ is given by,

$$|\Delta(t)| = \cos^{-1}\left[\frac{\hat{V} \times \hat{D}(t) \cdot \hat{V} \times \hat{S}(t)}{|\hat{V} \times \hat{D}(t)|\ |\hat{V} \times \hat{S}(t)|}\right]$$

But since, $\hat{V} \times a\hat{V} \equiv 0$

$$\hat{V} \times \hat{D}(t) \cdot \hat{V} \times \hat{S}(t) = \hat{V} \times \hat{D}_{t_o} \cdot \hat{V} \times \hat{S}_{t_o} \tag{70}$$

and Δ is not dependent upon time in the interval $t-t_o$.

The initial orientation of the RV can be fixed by specifying the azimuth coordinate of $\hat{L}$ at the initial time, t_o. RV rotation then causes the azimuth to change as the RV descends. If the rotation is counter-clockwise as viewed from the nose of the RV (right-hand screw rotation), the azimuth of $\hat{D}$ and $\hat{S}$ decreases, while if the RV rotation is clockwise as viewed from the RV nose (left-hand screw rotation), the azimuth of $\hat{D}$ and $\hat{S}$ increases. These considerations are summarized in,

$$\phi_D(t) = \phi_D(t_o) \pm W_{RV}\,(t-t_o) \qquad \begin{cases} + \text{ LHS} \\ - \text{ RHS} \end{cases} \tag{42}$$

$$\phi_S(t) = \phi_D(t) - \Delta \tag{43}$$

which appeared in the previous text.

APPENDIX B

RELATIVE GAIN OF RECEIVING ARRAY

The purpose of this Appendix is to derive the gain of a planar phased array antenna in the (ϕ, θ) direction (see Figure 24) relative to the (ϕ_o, θ_o) direction to which, it is assumed, the array is electronically steered.

If the elements are arranged in N columns spaced at intervals of Δy, and M rows spaced at intervals of Δz, the element position vectors for this rectangular array lattice are given by,

$$\left.\begin{aligned} \vec{R}(n, m) &= n\,\Delta y\,\hat{y}\; m\,\Delta z\,\hat{z} \\ n &= 0, 1, 2 \ldots N-1 \\ m &= 0, 1, 2 \ldots M-1 \end{aligned}\right\} \tag{71}$$

with respect to the origin in the lower left corner of the antenna as depicted in Figure 24.

A plane wave incident from the (ϕ, θ) direction has a wavevector $\vec{k}$ whose components are proportional to the direction cosines of $\vec{k}$, COS α and COS β, with respect to the $\hat{y}$ and $\hat{z}$ directions, respectively:

$$\vec{k} = k_y\,\hat{y} + k_z\,\hat{z} = \frac{2\pi}{\lambda}\,(\cos\alpha\,\hat{y} + \cos\beta\,\hat{z}) \tag{72a}$$

$$\left.\begin{aligned} \cos\alpha &= \cos\theta\,\sin\phi \\ \cos\beta &= \sin\theta \end{aligned}\right\} \tag{72b}$$

On the other hand the array is phased to maximize the gain for a plane wave with wavevector $\vec{k}_o$ given by,

IA – 62, 216

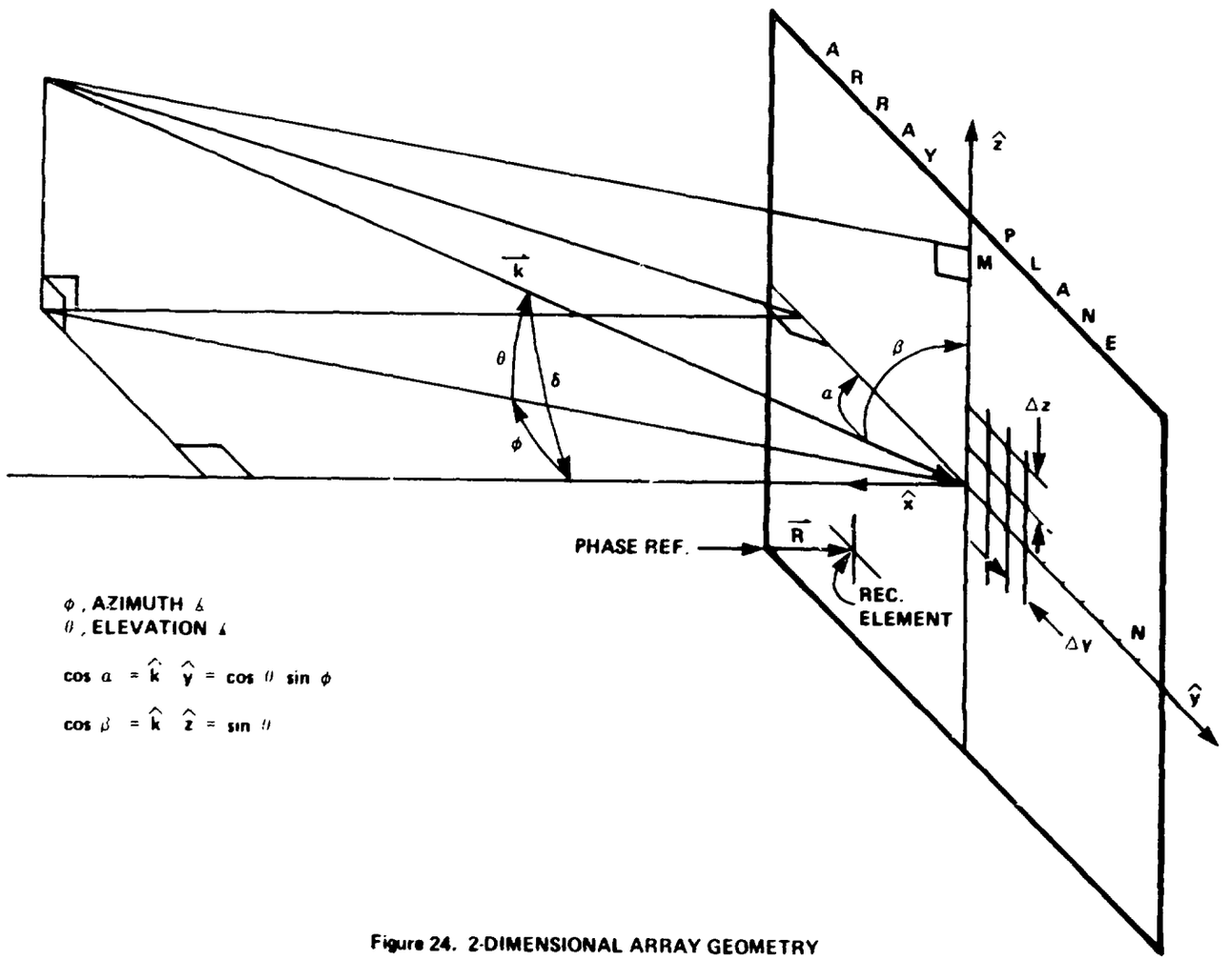

ϕ, AZIMUTH ∠
θ, ELEVATION ∠

$\cos\alpha = \hat{k}\ \hat{y} = \cos\theta \sin\phi$

$\cos\beta = \hat{k}\ \hat{z} = \sin\theta$

Figure 24. 2-DIMENSIONAL ARRAY GEOMETRY

$$\vec{k}_o = k_{y_o}\,\hat{y} + k_{z_o}\,\hat{z} = \frac{2\pi}{\lambda}\,(\cos\alpha_o\,\hat{y} + \cos\beta_c\,\hat{z}) \tag{73a}$$

$$\left.\begin{aligned} \cos\alpha_o &= \cos\theta_o \sin\phi_o \\ \cos\beta_o &= \sin\theta_o \end{aligned}\right\} \tag{73b}$$

Therefore, the phase angle by which the wave represented by $\vec{k}$ differs from the optimum phase at element (n, m) is given by,

$$\phi_{\Delta k}(n, m) = \Delta k \cdot \vec{R}(n, m) \tag{74}$$

$$= \frac{2\pi}{\lambda}\left[n\,\Delta y(\cos\alpha - \cos\alpha_o) + m\,\Delta z(\cos\beta - \cos\beta_o)\right]$$

and the total amplitude of the contribution to the array output from $\vec{k}$, relative to that at $\vec{k}_o$ is given by,

$$\frac{A(k)}{A(k_o)} = \left|\frac{\sum_{n=0}^{N-1}\sum_{m=0}^{M-1} e^{i\phi_{\Delta k}(n,m)}}{\sum_{n=0}^{N-1}\sum_{m=0}^{M-1} e^{io}}\right|$$

$$= \left|\frac{\sum_{n=0}^{N-1} e^{i\frac{2\pi m\Delta y}{\lambda}(\cos\alpha - \cos\alpha_o)} \sum_{m=0}^{M-1} e^{i\frac{2\pi m\Delta z}{\lambda}(\cos\beta - \cos\beta_o)}}{NM}\right| \tag{75}$$

in which uniform array illumination is implicit since all phasor amplitudes are unity. Addition of the geometric sums in Equation (75) and extraction of an unimportant phase factor yields,

$$\frac{A(k)}{A(k_o)} = \frac{\mathrm{SIN}\left[\frac{A\pi}{\lambda}(\cos\alpha-\cos\alpha_o)\right]\ \mathrm{SIN}\left[\frac{B\pi}{\lambda}(\cos\beta-\cos\beta_o)\right]}{N\,\mathrm{SIN}\left[\frac{A\pi}{N\lambda}(\cos\alpha-\cos\alpha_o)\right]\ M\ \mathrm{SIN}\left[\frac{B\pi}{M\lambda}(\cos\beta-\cos\beta_o)\right]} \tag{76}$$

in which,

$$A = N\Delta y \tag{77a}$$

is the array length, and

$$B = M\Delta z \tag{77b}$$

is the array width. In addition to the result expressed by Eq. (76), it should be noted that the gain of an array in a particular direction is approximately proportional to the array aperture projected in a plane perpendicular to that direction. The projection factors for a unit of array area are the direction cosines of $\vec{k}_o$ and $\vec{k}$ with respect to $\hat{x}$, i.e.,

$$\hat{k}_o \cdot \hat{x} = \cos\ \delta_o = \cos\theta_o \cos\phi_o \tag{78}$$

$$\hat{k} \cdot \hat{x} = \cos\ \delta = \cos\theta \cos\phi \tag{79}$$

The gain at $\vec{k}$ relative to $\vec{k}_o$ is finally given by,

$$g_{REL}\ (k,k_o) = \left[\frac{A(k)}{A(k_o)}\right]^2 \frac{\cos\delta}{\cos\delta_o} \tag{80}$$

It should be remembered that Equation (76) is obtained for an assumption of uniform illumination and is based on an "array factor" calculation which does not take into account the individual "embedded" element patterns.